KINEMATIC CALIBRATION OF INDUSTRIAL ROBOTS USING FULL POSE MEASUREMENTS AND OPTIMAL POSE SELECTION

A THESIS SUBMITTED TO
THE GRADUATE SCHOOL OF NATURAL AND APPLIED SCIENCES
OF
MIDDLE EAST TECHNICAL UNIVERSITY

BY

BERK YURTTAGÜL

IN PARTIAL FULFILLMENT OF THE REQUIREMENTS
FOR
THE DEGREE OF MASTER OF SCIENCE
IN
MECHANICAL ENGINEERING

DECEMBER 2010

Approval of the thesis:

KINEMATIC CALIBRATION OF INDUSTRIAL ROBOTS USING FULL POSE MEASUREMENTS AND OPTIMAL POSE SELECTION

submitted by **BERK YURTTAGÜL** in partial fulfillment of the requirements for the degree of **Master of Science in Mechanical Engineering Department, Middle East Technical University** by,

Prof. Dr. Canan ÖZGEN _____
Dean, Graduate School of **Natural and Applied Sciences**

Prof. Dr. Süha ORAL _____
Head of Department, **Mechanical Engineering**

Asst. Prof. Dr. E. İlhan KONUKSEVEN _____
Supervisor, **Mechanical Engineering Dept., METU**

Examining Committee Members:

Prof. Dr. Kemal ÖZGÖREN
Mechanical Engineering Dept., METU _____

Asst. Prof. Dr. E. İlhan KONUKSEVEN
Mechanical Engineering Dept., METU _____

Prof. Dr. Tuna BALKAN
Mechanical Engineering Dept., METU _____

Asst. Prof. Dr.Buğra KOKU
Mechanical Engineering Dept., METU _____

Asst. Prof. Dr. Afşar SARANLI
Electrical and Electronics Engineering Dept., METU _____

Date: _____

I hereby declare that all information in this document has been obtained and presented in accordance with academic rules and ethical conduct. I also declare that, as required by these rules and conduct, I have fully cited and referenced all material and results that are not original to this work.

Name, Last Name: BERK YURTTAGÜL

Signature :

ABSTRACT

KINEMATIC CALIBRATION OF INDUSTRIAL ROBOTS USING FULL POSE MEASUREMENTS AND OPTIMAL POSE SELECTION

Yurttagül, Berk
M.S., Department of Mechanical Engineering
Supervisor : Asst. Prof. Dr. E. İlhan KONUKSEVEN

December 2010, 70 pages

This study focuses on kinematic calibration of industrial robots. Kinematic modeling, parameter identification and optimal pose selection methods are presented. A computer simulation of the kinematic calibration is performed using generated measurements with normally distributed noise. Furthermore, kinematic calibration experiments are performed on an ABB IRB 6600 industrial robot using full pose measurements taken by a laser tracking system. The kinematic model of the robot is developed using the modified Denavit - Hartenberg convention. A nonlinear least-squares method is employed during the parameter identification stage. According to the experiment results, the initial robot positioning errors are reduced by more than 80%.

Keywords: Kinematic Calibration, Parameter Identification, Industrial Robots

ÖZ

ENDÜSTRİYEL ROBOTLARIN TAM POZ ÖLÇÜMLERİ VE ENİYİLENMİŞ POZLAR KULLANILARAK KİNEMATİK KALİBRASYONU

Yurttagül, Berk
Yüksek Lisans, Makine Mühendisliği Bölümü
Tez Yöneticisi : Yrd. Doç. Dr. E. İlhan KONUKSEVEN

Aralık 2010, 70 sayfa

Bu çalısma endüstriyel robotların kinematik kalibrasyonu üzerine odaklanmaktadır. Kinematik modelleme, parametre tanılama ve en iyi poz seçimi yöntemleri sunulmaktadır. Üretilen normal dağılımlı gürültü içeren ölçümler kullanılarak bilgisayar ortamında kinematik kalibrasyon benzetimleri elde edildi. Bunun yanı sıra, tam poz ölcümleri kullanılarak ABB IRB 6600 endüstriyel robotu üzerinde kinematik kalibrasyon deneyleri gerçekleştirildi. Robotun kinematik modeli değiştirilmiş Denavit - Hartenberg notasyonu kullanılarak oluşturuldu. Parametre tanılama işleminde doğrusal olmayan küçük kareler yöntemi kullanıldı. Deney sonuçlarına göre robot konumlanma hataları %80 oranında azaltıldı.

Anahtar Kelimeler: Kinematik Kalibrasyon, Parametre Tanılama, Endüstriyel Robotlar

To Sinan, Mine and Melis..

ACKNOWLEDGMENTS

First and foremost, I would like to thank to my advisor Asst. Prof. Dr. E. İlhan Konukseven for his guidance and direction throughout this research. I also would like to thank Prof. Dr. Tuna Balkan for his enlightening comments that guide me on the right path. Cenker Berk and Kübra Çelikkaya helped obtaining the measurements and provided the necessary tools for this study, many thanks. My fellow labmates in Virtual Reality Laboratory: Alican Tabakçı, Serter Yılmaz, Özgür Başer and Gökhan Bayer provided companionship during the whole period of the study for which I am grateful. Murat Bilen supported the study with his vision and knowledge on the subject. Last but not least, I dedicate my thesis to my family for their love and endless support.

TABLE OF CONTENTS

LIST OF TABLES

TABLES

LIST OF FIGURES

FIGURES

CHAPTER 1

INTRODUCTION

Following the first installed industrial robot developed by Devol and Engelberger in 1961, the use of industrial robots rapidly increased and they quickly became an indispensable part of the manufacturing especially in the automotive industry. Today, they are used in a wide range of applications and are capable of performing the difficult tasks they are programmed for.

The most common method of robot programming is performed on the factory floor by manually teaching the robot the required poses of the task. While this method is tedious and even hazardous in some cases, it benefits from the robot's ability to successfully repeat a previous instruction, a known quality of the industrial robots. On the other hand, emerging programming methods make it possible to create robot tasks in a virtual environment without interrupting the production cycle. While these new methods are proved to be less tiresome and more efficient, they require the robot to be able to move to an instructed pose accurately. This requirement put the robot's accuracy into the spotlight.

The call for improving the accuracy of a robot without a redesign gave rise to the robot calibration techniques. Robot calibration is being studied extensively for the last twenty-five years, during which time, several studies have been conducted for better understanding the error sources on robots and different methods have been proposed accordingly. However, in an industrial point of view, a robot calibration method should not only be effective but also should be efficient in terms of the time, effort and cost to be invested.

In this study, a rapid and an effective approach to the industrial robot calibration is sought. According to this, the previous studies on the subject have been reviewed. A computer code featuring a graphical user interface is developed to be used for both the simulations and the calibration experiments. A novel and highly accurate measurement system is used to evaluate

the success of the calibration using additional measurements. Furthermore, an optimal pose selection algorithm is used to obtain the poses amongst the gathered measurements in terms of suppressing the measurement noise.

The pose error of a typical industrial robot and the part associated with the geometric parameters are inspected. Moreover, the effects of the measurement noise and the quality of the measurements on the improvement of the accuracy of an industrial robot as a result of the kinematic calibration are evaluated by simulations. The inverse geometric model is developed to apply the error correction methods.

According to the results of the research and by using the selected methods, the necessary computer tools along with graphical user interfaces are created which enable a progressive kinematic calibration that can be used on a range of industrial robots on the factory environment. These developed computer tools are further tested on calibration experiments which are proved to be efficient.

1.1 Objectives

The main objectives are:

- To investigate the robot calibration methods for their efficiency and to determine an approach to be taken to calibrate industrial robots.
- To code the mathematical routines and to design graphical user interfaces to be used during the simulations and the robot calibration procedure.
- To simulate the robot calibration using the designed tools and the generated measurements with normally distributed noise.
- To perform robot calibration experiments and to evaluate the errors associated with the nominal robot model.
- To evaluate the accuracy improvement of the robot as a result of the calibration using the selected measurements.

1.2 Outline of the Thesis

Chapter 2 presents background information on robot calibration and reviews the related works on the subject by presenting the approach and the techniques used on each step of the robot calibration. The modeling methods used in the study and their implementation on the robot under study are presented is Chapter 3. The details of the parameter identification and the pose selection method are discussed in Chapter 4. The details of the simulations and their results are presented at Chapter 5. The experiment on an industrial robot and its results are presented in Chapter 6. The reached conclusions and the future work are discussed in Chapter 7.

CHAPTER 2

REVIEW OF ROBOT CALIBRATION METHODS

This chapter reviews the existing methods of robot calibration. The related information on the subject like robot programming, performance evaluation and sources of error are given. The previous works on the literature is also presented.

2.1 Robot Error Sources and Performance Evaluation

The performance requirements for industrial robots differ by the task they perform. The two most frequently used performance criteria and their effect on different programming techniques are discussed in the next sections.

2.1.1 Accuracy and Repeatability

The accuracy and the repeatability of an industrial robot are largely used to evaluate its performance of reaching a desired pose. Repeatability is defined as the ability of the robot to reach the same taught position while accuracy is defined as the ability of the robot to precisely reach a programmed position [1]. Figure 2.1 shows the difference between the effect of accuracy and repeatability on the final position of the robot's end effector.

Many factors credited to affect the overall robot accuracy including but not limited to deviations from nominal geometric parameters, joint offsets, link and joint compliance, gear trains, gear backlash, gear runout and thermal factors [2, 3, 4, 5, 6]. The errors in geometric parameters are mainly due to the tolerances in manufacturing and the assembly of the robots' parts. The flexibility of robot joints and the link deflection under self-gravity and load are

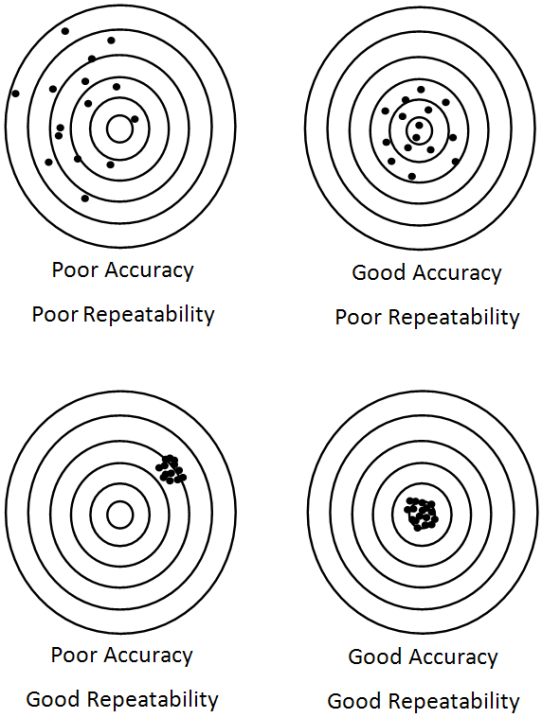

Figure 2.1: The effect of accuracy and repeatability [4].

attributed to compliance errors while thermal distortion and expansions of robot components are attributed to thermal errors [7].

The robot pose errors are more generally divided into geometric and non-geometric errors [2]. Geometric errors are caused by factors like joint offsets and deviations from the nominal geometric parameters. Non-geometric errors are caused by other factors like joint and link compliance, friction and clearance.

2.1.2 Programming

There are two common methods to program an industrial robot: online programming and offline programming. The online programming of industrial robots involves teaching the robot a sequence of poses manually, usually using a teach pendant, which all together compose a specific task. Another method is to design the task using separate software and then load it to the robot's controller, which is known as offline programming. The visual robot simulation programs and the production stops due to the time it takes to program each robot online make

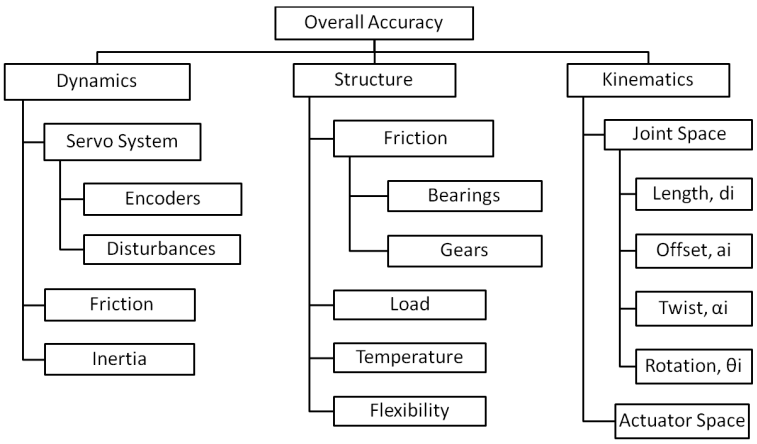

Figure 2.2: Factors effecting the robot accuracy and repeatability. [4]

the latter method a better alternative. While the former method depends very much on the repeatability, a characteristic that is known to be adequately high on today's industrial robots, the latter relies more on the accuracy of the industrial robots [3, 8]. In other words, for offline programming methods to be applicable, the robot model that is used offline must accurately describe the actual robot.

2.2 Robot Calibration

Robot calibration is a process that improves the accuracy of a robot by identifying a more accurate functional relationship between the nominal and the actual robot [5]. The aim of robot calibration is to improve the accuracy to reach the repeatability of the robot by modifications through software.

Bernhardt and Albright classified the robot calibration into two types [9]: static and dynamic calibration (Figure 2.3). Static calibration aims to identify the parameters that affect the static positioning characteristics of the robot like link lengths, joint offsets, gear runout, gear backlash, actuator and link elasticity and coupling factor. Dynamic calibration, on the other hand, deals with the identification of parameters that effect motion characteristics of the manipulator like friction and the mass and the stiffness of the links and the actuators.

A more general classification is made by Roth, Mooring and Ravani where they divided the robot calibration into three levels [5]: Level 1 is a joint level calibration which determines the

joint offset errors. Level 2 is an entire robot kinematic model calibration which determines the basic kinematic geometry of the robot and the joint angle relationships. Finally, Level 3 is a non-kinematic calibration which determines the dynamic model of the robot.

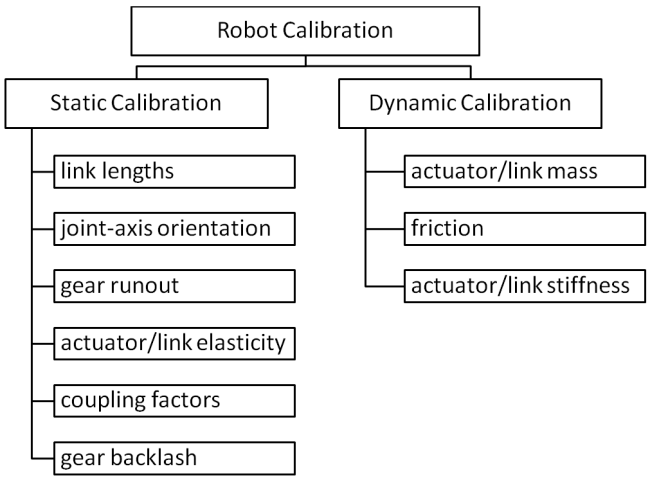

Figure 2.3: Static and dynamic calibration classification of Bernhardt and Albright. [9]

In general, robot calibration is divided into four steps [5]:

- Modeling
- Measurements
- Identification
- Verification and Correction

2.2.1 Modeling

The first step of robot calibration is to establish a model that accurately maps the joint values to the end-effector pose. Everett and later Schroer identified the three requirements for this model to be used on the parameter identification stage as minimality, completeness and model continuity or proportionality [10, 11, 12].

Minimality refers to the use of minimal number of parameters by the kinematic model. Completeness is the ability of the model to map joint values into end-effector positions for all

arbitrary manipulators. Model continuity or proportionality requires small changes in the robot geometry to result small changes on the model parameters.

In an ideal case, this model accounts for all the factors that affect the robot pose errors. However, Mooring and Padavala argued that the effort associated with the more complex model is not justified if it improves just a small amount of the resulting robot accuracy [13]. Furthermore, a good number of studies show that the geometric factors have much greater influence on robot pose accuracy [3, 4, 7, 8, 13, 14, 15, 16].

The first study to include the non-geometric parameters to the calibration model is by Whitney et al. which they used a model with geometric parameters as well as non geometric parameters like joint compliance, backlash and gear transmission errors and calibrated a PUMA 560 robot using this model. Veitschegger and Wu calibrated a PUMA 560 robot by using position measurements to identify the geometric parameters and showed that the positioning errors are greatly reduced after the calibration [17]. Judd and Kasinski found out on their study with two AID-900 robots that the joint angle offsets were accountable for nearly 90% of the total rms error, deviations from nominal link parameters were accountable for a futher 5% and gearing errors were only accountable for 1% of the total rms error [3]. Mooring and Padavela calibrated a PUMA 560 robot using four different models with increasing complexity [13]. They reduced the initial mean positioning error of five poses from 30.04 mm to 0.47 mm with a model consisting geometric parameters and joint offsets and to a further 0.42 mm by adding compliance to this model. Caenen and Angue improved the mean accuracy of a TH8 robot from 2.82 mm to 0.69 mm by only identifying the geometric parameters and to a further 0.58 mm by identifying the non-geometric parameters associated with compliance [15]. On their studies with Puma 760, Chen and Chao reduced the mean error distance of 5.9 mm to about 1 mm using geometric parameters and to an additional 0.28 mm by adding non-geometric parameters to characterize the twist angles in the second and the third joints and the backlash in third joint due to the gravitational effects [16]. Bernhardt showed the effect of identifying additional parameter classes on the positioning errors of a typical spot welding robot [14] (Figure 2.4). Gong et al. reduced the mean residual error of 30 positions from 1.059 mm to 0.126 mm by identifying only the geometric parameters and to a further 0.088 mm after calibrating for compliance errors of the second and the third joints [7]. After calibrating for these geometric and non-geometric errors, they also established and applied empirical thermal error models to estimate thermal errors by monitoring the temperature field

at different operating conditions [7]. Jang et al. calibrated a DR06 robot for the geometric errors in addition to the non-geometric joint angle deformations resulting from a payload by dividing the robot workspace into several local regions and interpolating the identified errors of each local region to obtain continuous functions of joint angles in the workspace [18]. More recently, Gatla et al. calibrated a Staubli RX-130 robot by using only geometric parameters which improved the robot's mean deviation of aiming a laser at a fixed point from 5.64 mm to 1.05 mm [8]. Lightcap, Hamner, Schmitz and Banks employed a two level optimization algorithm to identify the geometric and flexibility parameters of a PA10-6CE robot using measurements from a CMM where they reduced the positioning errors by 50 - 80% [19].

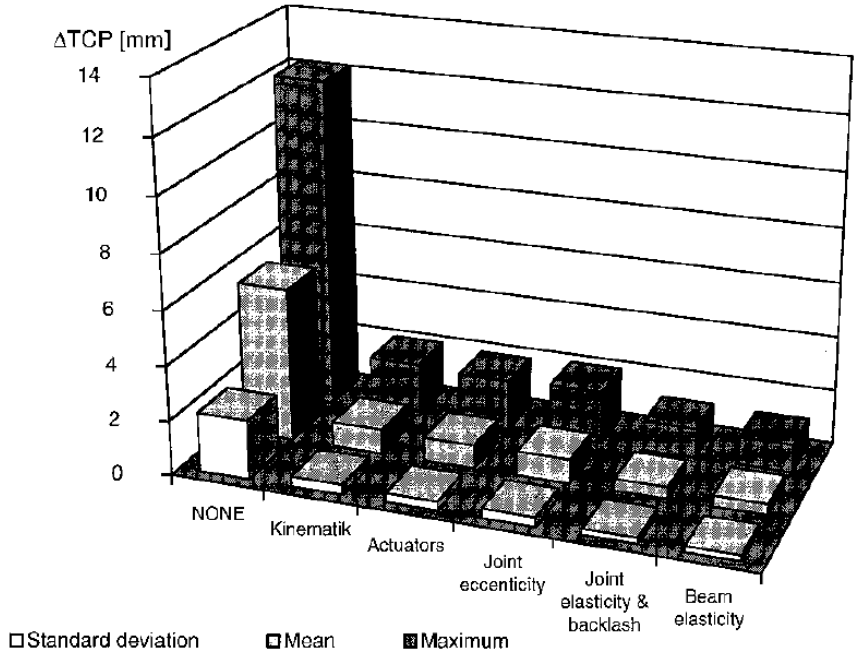

Figure 2.4: Reduction of positioning error ΔTCP when identifying additional parameter classes from none to full model [14].

Due to the results of these studies showing higher improvements in accuracy by just identifying the geometric parameters and also the complexity of adding the non-geometric parameters to the model, non-geometric factors are mainly discarded or neglected on the literature. The main idea behind it is, -baring the errors caused by non-geometric factors- robot accuracy can be greatly improved by identifying the geometric parameters of the robot. Moreover, since most robot controllers use geometric parameters on their model, it is easier to correct these parameters to improve the robot accuracy. This approach of identifying only the geometric

parameters is identical to the Level 2 calibration of Roth, Mooring and Ravani and it is still largely used.

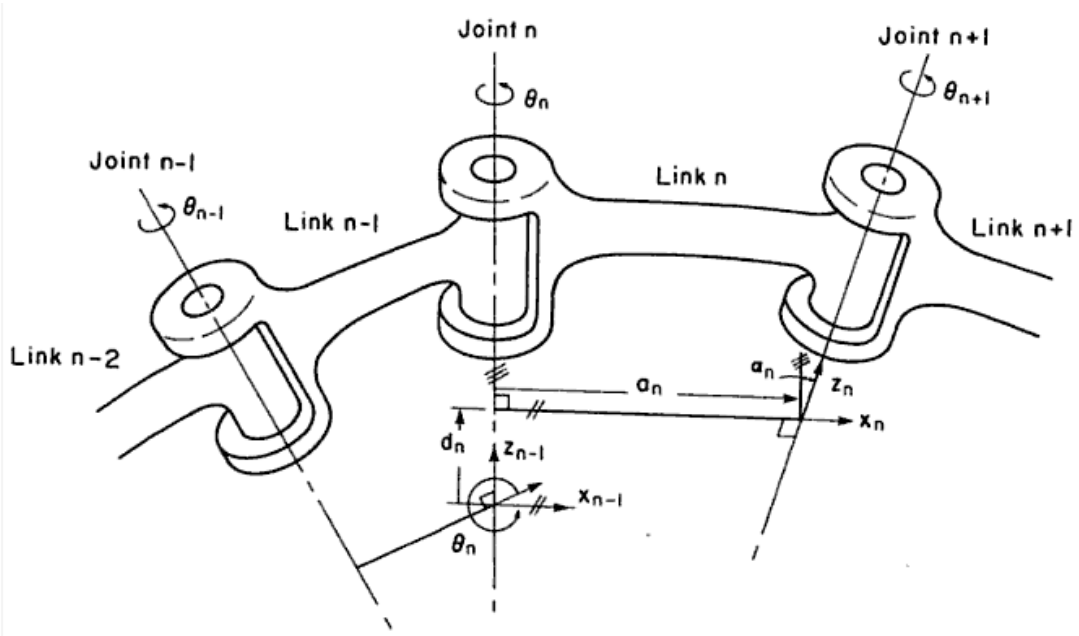

Figure 2.5: Denavit - Hartenberg parameters. [20]

The most widely used method of kinematic modeling is proposed by Denavit and Hartenberg where homogenous transformation matrices are used to represent the relationship between two consecutive link coordinate frames using four parameters [21] (Figure 2.5). These transformation matrices are then multiplied to create a transformation between the base and the end-effector coordinate systems. However, it has been shown by Hayati and Mirmirani that when two consecutive joint axes are parallel or nearly parallel, Denavit - Hartenberg model violates the model continuity or proportionality property since small changes in the robot geometry does not result small changes on the model parameters [22]. To overcome this, they introduced an alternative parameterization to be used in case of parallel or nearly parallel adjacent joint axes.

Alternative modeling techniques are also employed in robot calibration. Robertson and Dumont used genetic programming to obtain physical models by using mathematical operators that evolved to the equations based on the measurements taken from the robot [23]. Dolinsky et al. also used genetic programming to obtain evolved symbolic expressions of joint cor-

rection models for the first three joints of a PUMA 761 robot [24]. They reduced the mean positioning error of the robot with this method from 1.85 mm to 0.77 mm.

It should also be noted that all of the studies discussed so far employ parametric models and thus can be considered model-based approaches. There are also non-parametric or modeless methods where the errors are approximated by using the measured data. An example to this is the method proposed by Wang and Bai which uses a neural network algorithm to estimate the positioning errors from the measured errors of the grids on a calibration board [25].

2.2.2 Measurements

The second step of robot calibration is obtaining the required data from the robot under study. This data should be suitable to the model, in a sense, to relate the input of the established model to the output [5].

Measurement systems used in the robot calibration have great importance in terms of identifying the model parameters and evaluating the robot performance. They should meet the requirements of the calibration process in terms of accuracy and effectiveness. The measurement systems used in the previous robot calibration studies include laser trackers [7, 26], optical [8], photogrammetric [8, 18, 25, 27] and mechanical [24] systems, coordinate measuring machines [13, 19] and theodolites [2, 16].

Hidalgo and Brunn showed that these measurement systems differ from each other not only by their techniques but also by their characteristics like cost, sampling rate, set-up time, nominal accuracy and repeatability [28]. They also showed that high cost systems do not necessarily have higher accuracy, repeatability or resolution. Clearly, the most important properties are accuracy and repeatability, but an ideal measurement system should also cost less and require minimum amount of time to set-up. While most of the previous studies use optical and photogrammetric systems, laser tracking systems are more frequently used in the industry for their higher accuracy than their low-cost counterparts.

It should be noted that not all robot calibration methods require external measurement systems. Khalil et al. compared different geometric parameter calibration methods that use an external measurement device or the joint encoder readings alone to identify the geometric parameters [29]. The latter methods are considered as self-calibration methods on their study

which use specific constraints like the terminal link being on the same pose (or position) or on the same plane for the chosen configurations.

2.2.3 Identification

The third step is to identify the parameters of the model using the gathered data. The most common methods used in this stage are formulated as regression problems to determine the parameters that minimize the error between the model and the measured data. Gauss-Newton algorithm is used for nonlinear models for it quickly converges provided that the initial estimates are close enough to the solution [30, 31]. This algorithm uses linear Taylor expansion of the nonlinear model and then employs ordinary least squares iteratively.

However, Gauss-Newton algorithm is known to perform poorly in case of singular or ill-conditioned matrices due to unidentifiable parameters, insufficient measurements and/or poor scaling issues [30, 31]. Levenberg - Marquardt algorithm [32, 33], a modified version of the Gauss-Newton algorithm, is a more robust choice in these cases.

Search algorithms can also be used on this stage but they are unavoidably slower. An example to this is the study by Liu et.al where they used genetic algorithm in their simulations to identify the geometric parameters of a PUMA 560 robot [34].

A lot of research on this step focuses on optimally selecting the measurement configurations to improve the performance of the identification. This is stated as the problem of determining a set of reachable robot measurement configurations that minimizes the effect of measurement noise on the identification of robot kinematic parameters [35]. These measurements are selected by using an observability index based on the identification Jacobian matrix. Driels and Pathre proposed to use the condition number of the identification Jacobian [36] while Borm and Menq proposed the geometric mean of all the singular values of the identification Jacobian as the observability index [37]. Nahvi and Hollerbach proposed the minimum singular value and also the square of smallest non-zero singular value divided by the largest singular value of the identification Jacobian as observability indices [38, 39]. These observability indices are reviewed by Sun and Hollerbach where they relate them to the alphabet optimalities of the experimental design literature [39].

The methods used in finding the optimal measurements using the observability index also dif-

fer. Zhuang et.al proposed the use of the simulated annealing and later genetic algorithm on selecting the optimum measurements arguing that gradient-based methods frequently trapped into local minima [35, 40]. Sun and Hollerbach proposed a method called active robot calibration algorithm based on DETMAX algorithm of Mitchell [41] but using determinant-based updating observability index instead of an eigenvalue-based one [42]. Watanabe et al. proposed an automatic calibration method that determines the poses to be measured based on their condition number [27]. It should also be noted that Khalil and Besnard pointed out that randomly selected measurements generally have sufficient condition number [29].

2.2.4 Verification and Correction

The final step of robot calibration is correcting the errors of the robot. The simplest way to do this is by updating the identified parameter values inside the robot controller. However, most robot controllers employ only the geometric parameters on their model. Furthermore, not all robot controllers allow the nominal model parameters to be changed. Another method is to change the robot program by updating the robot targets of the task. This requires the inverse model of the robot to generate so-called fake targets. A final way is using an external unit to correct the errors real time.

It is also a good practice to validate the accuracy of the identification prior to the correction procedure. Since the identification algorithms use the supplied measurement data for estimating the model parameters, additional measurements should be obtained from the robot to verify these estimated parameters. This will also help to have a basic idea on the pose errors before and after the calibration.

CHAPTER 3

KINEMATIC MODELING

This chapter presents the information on kinematic modeling of the IRB 6600 robot used during the study. The mathematical background on the kinematic modeling and the modeling of the robot under study are discussed in detail.

3.1 Mathematical Background

This section presents the representation of position and orientation, homogenous transformation and the geometric representation of serial-link robots, specifically method of Denavit and Hartenberg. The sources used during this chapter are [6, 31, 43].

3.1.1 Representation of Position and Orientation

3.1.1.1 Position

The 3x1 position vector:

$$^{\mathrm{A}}P_{\mathrm{B}} = \begin{bmatrix} p_{\mathrm{x}} \\ p_{\mathrm{y}} \\ p_{\mathrm{z}} \end{bmatrix} \tag{3.1}$$

represents the position of the origin of the coordinate frame A relative to coordinate frame B [31, 43]. The components p_x, p_y and p_z of this vector are the Cartesian coordinates of the origin of the coordinate frame A in the B frame.

3.1.1.2 Orientation

Let the unit vectors giving the principal directions of coordinate system B denoted as $\hat{x}_B$, $\hat{y}_B$, $\hat{z}_B$. They can be written in terms of the coordinate system A as ${}^A\hat{x}_B$, ${}^A\hat{y}_B$, ${}^A\hat{z}_B$. These three unit vectors can be stacked on the columns of a 3x3 matrix:

$$ {}^AR_B = \begin{bmatrix} {}^A\hat{x}_B \\ {}^A\hat{y}_B \\ {}^A\hat{z}_B \end{bmatrix} = \begin{bmatrix} \hat{x}_B.\hat{x}_A & \hat{y}_B.\hat{x}_A & \hat{z}_B.\hat{x}_A \\ \hat{x}_B.\hat{y}_A & \hat{y}_B.\hat{y}_A & \hat{z}_B.\hat{y}_A \\ \hat{x}_B.\hat{z}_A & \hat{y}_B.\hat{z}_A & \hat{z}_B.\hat{z}_A \end{bmatrix} \tag{3.2} $$

which is called the rotation matrix. The rotation of the frame A through an angle θ about the $\hat{x}_B$ axis is:

$$ R_x(\theta) = \begin{bmatrix} 1 & 0 & 0 \\ 0 & cos\theta & -sin\theta \\ 0 & sin\theta & cos\theta \end{bmatrix} \tag{3.3} $$

about the $\hat{y}_B$ axis is:

$$ R_y(\theta) = \begin{bmatrix} cos\theta & 0 & sin\theta \\ 0 & 1 & 0 \\ -sin\theta & 0 & cos\theta \end{bmatrix} \tag{3.4} $$

and about the $\hat{z}_B$ axis is:

$$ R_z(\theta) = \begin{bmatrix} cos\theta & -sin\theta & 0 \\ sin\theta & cos\theta & 0 \\ 0 & 0 & 1 \end{bmatrix} \tag{3.5} $$

3.1.2 Homogenous Transformation

Homogenous transformation combines the position and the orientation.

$$ {}^BT_A = \begin{bmatrix} {}^BR_A & {}^BP_A \\ 0 & 1 \end{bmatrix} \tag{3.6} $$

The homogeneous transformation of a translation along an axis is denoted Trans. According to this, the translation of l along the $\hat{x}$ axis can be written as:

$$ Trans(\hat{x}, \theta) = \begin{bmatrix} 0 & 0 & 0 & l \\ 0 & 0 & 0 & 0 \\ 0 & 0 & 0 & 0 \\ 0 & 0 & 0 & 1 \end{bmatrix} \tag{3.7} $$

The homogeneous transformation of a rotation about an axis is denoted by Rot. According to this, the rotation through an angle θ about the $\hat{x}$ axis can be written as:

$$Rot(\hat{x}, \theta) = \begin{bmatrix} 1 & 0 & 0 & 0 \\ 0 & cos\theta & -sin\theta & 0 \\ 0 & sin\theta & cos\theta & 0 \\ 0 & 0 & 0 & 1 \end{bmatrix} \tag{3.8}$$

3.1.3 Geometric Representation

Denavit and Hartenberg introduced a widely adopted convention for assigning frames to the links of the robot [21]. A modified version of this convention by Khalil and Dombre is used throughout this research [6]. This convention has an advantage of using the same subscript for the parameters defining a transformation between two consecutive frames while it has a drawback of denoting link lengths with a parameter having the same index of the consecutive link.

The two main assumptions are: the links are perfectly rigid and the joints are ideal in a sense that there is neither backlash nor elasticity [6]. A serial robot is composed of a sequence of n-1 links and n joints where link 0 is the base of the robot and link n is the terminal link [6]. Joint i connects the link i to the link i-1 and its variable is denoted by θ_i [6]. A frame R_i is attached to each link i with [6]:

- The z_i axis is located along the axis of joint i.
- The x_i axis is located along the common normal between the z_i and z_{i+1} axis. If z_i and z_{i+1} axes are parallel or collinear, the choice of x_{i+1} is not unique. The intersection of x_i axis and z_i axes defines the origin O_i. If the joint axes intersect, the origin is at the point of intersection of the joint axes.
- The y_i axis is located using the right-hand rule to form (x_i,y_i,z_i) coordinate system.

The transformation matrix from frame R_{i-1} to frame R_i is expressed using the following four geometric parameters (Figure 3.1) [6]:

- Link twist: α_i is the angle between z_{i-1} and z_i about x_{i-1}

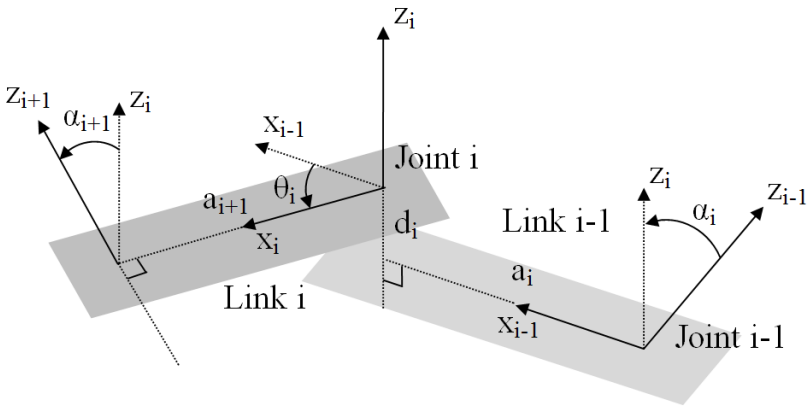

Figure 3.1: The parameters α_i, a_i, θ_i and d_i [31].

- Link length: a_i is the distance between z_{i-1} and z_i along x_{i-1}
- Joint angle: θ_i is the angle between x_{i-1} and x_i about z_i
- Link offset: d_i is the distance between x_{i-1} and x_i along z_i

And the transformation matrix defining the frame R_i relative to the frame R_{i-1} is:

$$
\begin{aligned}
{}^{i-1}T_i &= Rot(x,\alpha_i)Trans(x,a_i)Rot(z,\theta_i)Trans(z,d_i) \\
&= \begin{bmatrix} cos\theta_i & -sin\theta_i & 0 & a_i \\ cos\alpha_i sin\theta_i & cos\alpha_i cos\theta_i & -sin\alpha_i & -d_i sin\alpha_i \\ sin\alpha_i sin\theta_i & sin\alpha_i cos\theta_i & cos\alpha_i & d_i cos\alpha_i \\ 0 & 0 & 0 & 1 \end{bmatrix}
\end{aligned} \tag{3.9}
$$

As it is mentioned in the previous chapter, Denavit - Hartenberg representation faces a problem when two joint axes are parallel. When two consecutive joint axes i-1 and i are parallel, the x_{i-1} axis is chosen arbitrarily along one of the common normals between them. If z_i or z_{i-1} gets slightly misaligned, the common normal becomes uniquely defined and a big variation in the parameter d_{i-1} might occur [5, 6]. To overcome this problem, Hayati introduced a new parameter β_i representing a rotation around the y_{i-1} axis [22]. Thus, the general transformation matrix between two frames with consecutive parallel joints becomes [6] (Figure 3.2):

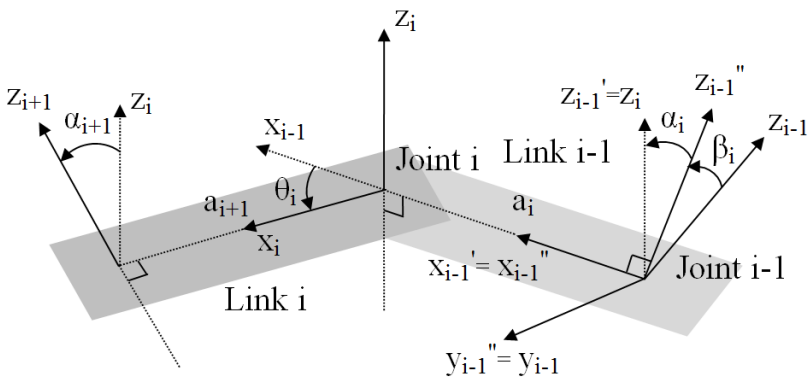

Figure 3.2: The additional parameter β_i for consecutive parallel joints. [31].

$$
{}^{i-1}T_i = Rot(y,\beta_i)Rot(x,\alpha_i)Trans(x,a_i)Rot(z,\theta_i)Trans(z,d_i) \tag{3.10}
$$

$$
= \begin{bmatrix} c\beta_i c\theta_i + s\alpha_i s\beta_i s\theta_i & s\alpha_i s\beta_i c\theta_i - c\beta_i s\theta_i & c\alpha_i s\beta_i & a_i c\beta_i + d_i c\alpha_i s\beta_i \\ c\alpha_i s\theta_i & c\alpha_i c\theta_i & -s\alpha_i & -d_i s\alpha_i \\ c\beta_i s\alpha_i s\theta_i - s\beta_i c\theta_i & s\beta_i s\theta_i + c\beta_i s\alpha_i c\theta_i & c\alpha_i c\beta_i & d_i c\alpha_i c\beta_i - a_i s\beta_i \\ 0 & 0 & 0 & 1 \end{bmatrix}
$$

where $c\gamma_i$ stands for $\cos\gamma_i$ and $s\gamma_i$ stands for $\sin\gamma_i$. In such cases, the parameter β_i is identified instead of d_i.

3.1.4 Forward Kinematics

The forward kinematics problem for a serial-chain manipulator is defined as finding the pose (position and orientation) of the end-effector relative to the base given the values of the joint variables and the geometric link parameters [31]. It can be solved by calculating the transformation between the frames fixed in the end-effector and in the base [31]. This transformation can be obtained by simply concatenating the transformations between the fixed frames of the adjacent links [31]:

$$
{}^{0}T_n = {}^{0}T_1\, {}^{1}T_2 \ldots {}^{n-2}T_{n-1}\, {}^{n-1}T_n \tag{3.11}
$$

3.1.5 Inverse Kinematics

The inverse kinematics problem for a serial-chain manipulator is defined as finding the values of the joint variables given the pose of the end-effector relative to the base and the geometric link parameters [31].

This problem can be solved algebraically or geometrically to obtain a closed-form solutions or using numerical methods. While closed-form solutions depend on the particular robot, they are faster than numerical solutions [31]. These solutions use particular geometric features like spherical wrist where three consecutive revolute joint axes intersect at a common point [31]. A closed-form solution of an industrial robot used in this study will be presented in the later sections.

3.2 Kinematic Modeling of ABB IRB 6600

This section presents the modeling of ABB IRB 6600 industrial robot.

3.2.1 Robot Description

ABB IRB 6600 industrial robot is selected as the robot of interest in this study. The version of the particular robot is 2.55 / 175. This version numbers represent that its maximum reach at wrist center is 2.55 meters and have a maximum handling capacity of 175 kg while it weighs 1.7 tons [44].

The positioning accuracy of the robot is reported on the production specification as 0.02 - 0.09 mm and the positioning repeatability is reported to as 0.08 - 0.18 mm [44]. The positioning accuracy of the calibrated robot is reported to be 97% within 1 mm with an average of 0.5 mm and a maximum value of 1.2 mm [44]. The joint axis resolution is reported as 0.001° - 0.005°.

ABB IRB 6600 industrial robot has six joint axes as shown in Figure 3.3. The type and the range of motion of these joint axes are shown in Table 3.1.

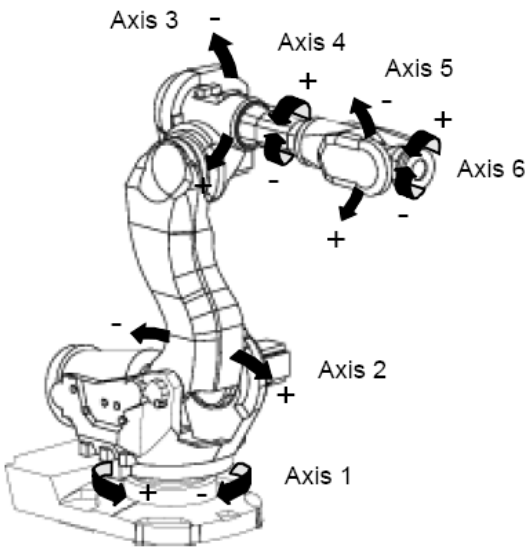

Figure 3.3: The six joint axes of the ABB IRB 6600 industrial robot [44].

Table 3.1: Type of motion and the range of movement of the six joints of the ABB IRB 6600 robot [44].

Joint Axis	Type of Motion	Range of Movement
1	Rotation motion	-180° to +180°
2	Arm motion	-65° to +85°
3	Arm motion	-180° to +70°
4	Wrist motion	-300° to +300°
5	Bend motion	-120° to +120°
6	Turn motion	-360° to +360°

3.2.2 Kinematic Modeling

The link lengths of the robot are shown in Figure 3.4. The modified Denavit - Hartenberg convention by Khalil and Dombre is used to attach the frames on each link and to represent the geometric link parameters of the robot [6]. The attached frames are shown in Figure 3.5.

3.2.2.1 Reference Frame

The base frame is assigned to be aligned with the first frame when θ_1=0, the same way it is defined on the robot controller as shown in Figure Figure 3.6. Since an external measurement

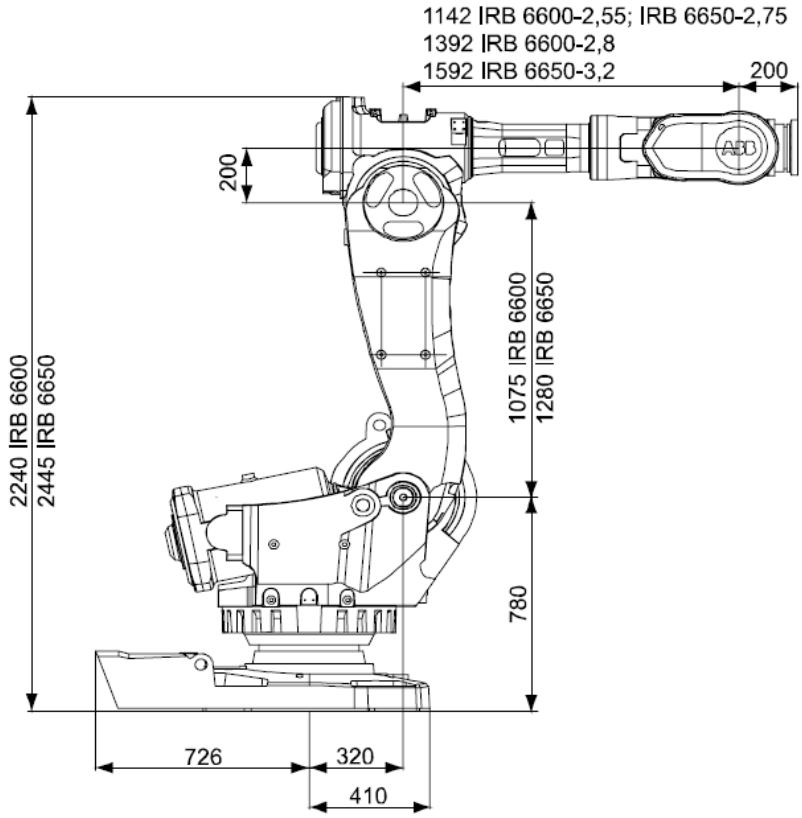

Figure 3.4: The description of the link lengths of the ABB IRB 6600 industrial robot [44].

system might obtain its measurements relative to a world reference frame, there is a need to define this reference frame. Six parameters are required to locate the robot base frame relative to a reference frame [6]:

$$^{R}T_0 = Rot(z,\gamma_R)Trans(z,b_R)Rot(x,\alpha_R)Trans(x,a_R)Rot(z,\theta_R)Trans(z,d_R) \tag{3.12}$$

Then, the transformation matrix from the reference frame to the first link frame becomes:

$$^{R}T_1 = Rot(z,\gamma_R)Trans(z,b_R)Rot(x,\alpha_R)Trans(x,a_R)Rot(z,\theta_R)Trans(z,d_R) \tag{3.13}$$
$$Rot(x,\alpha_1)Trans(x,a_1)Rot(z,\theta_1)Trans(z,d_1)$$

having α_1 and a_1 as zero, Eq. 3.14 can be written as:

$$^{R}T_1 = Rot(x,\alpha_0)Trans(x,a_0)Rot(z,\theta_0)Trans(z,d_0) \tag{3.14}$$
$$Rot(x,\alpha_1^{'})Trans(x,a_1^{'})Rot(z,\theta_1^{'})Trans(z,d_1^{'})$$

where α_0=0, a_0=0, $\theta_0=\gamma_R$, $d_0=b_R$, α_1'=α_R, a_1'= a_R, θ_1'=$\theta_1+\theta_R$ and d_1'= d_1+ d_R [6]. For simplicity, the parameters α_1', a_1', θ_1' and d_1' will be referred as α_1, a_1, θ_1 and d_1 respectively.

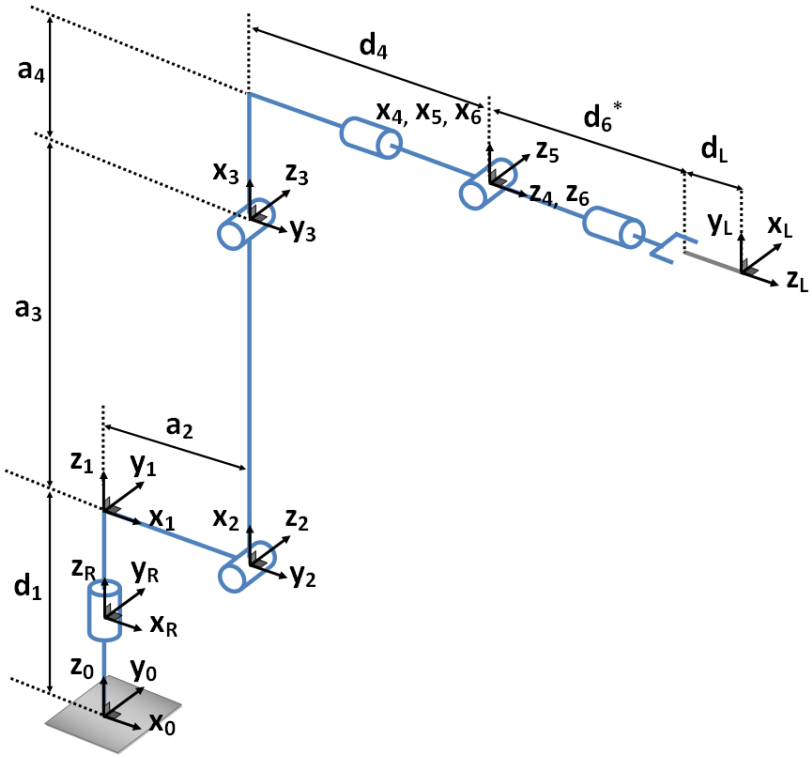

Figure 3.5: The attached frames for ABB IRB 6600 robot.

3.2.2.2 End-Effector Frame

The end-effector frame is assigned according to the mounting of T-Mac probe as shown in Figure 6.1. Six parameters are required to locate the end-effector frame relative to last link frame[6]:

$$^{6}T_{\mathrm{L}} = Rot(z,\gamma_{\mathrm{L}})Trans(z,b_{\mathrm{L}})Rot(x,\alpha_{\mathrm{L}})Trans(x,a_{\mathrm{L}})Rot(z,\theta_{\mathrm{L}})Trans(z,d_{\mathrm{L}}) \tag{3.15}$$

Then, the transformation matrix from the fifth link frame to the end-effector frame becomes:

$$\begin{aligned} ^{5}T_{\mathrm{L}} &= Rot(x,\alpha_6)Trans(x,a_6)Rot(z,\theta_6)Trans(z,d_6) \\ &Rot(z,\gamma_{\mathrm{L}})Trans(z,b_{\mathrm{L}})Rot(x,\alpha_{\mathrm{L}})Trans(x,a_{\mathrm{L}})Rot(z,\theta_{\mathrm{L}})Trans(z,d_{\mathrm{L}}) \end{aligned} \tag{3.16}$$

which can be written as:

$$\begin{aligned} ^{5}T_{\mathrm{L}} &= Rot(x,\alpha_6)Trans(x,a_6)Rot(z,\theta_6^{'})Trans(z,d_6^{'}) \\ &Rot(x,\alpha_{\mathrm{L}})Trans(x,a_{\mathrm{L}})Rot(z,\theta_{\mathrm{L}})Trans(z,d_{\mathrm{L}}) \end{aligned} \tag{3.17}$$

where θ_L'=θ_6+θ_L and d_L'= d_6+ d_L [6]. For simplicity, the parameters θ_L' and d_L' will be referred as θ_L and d_L respectively.

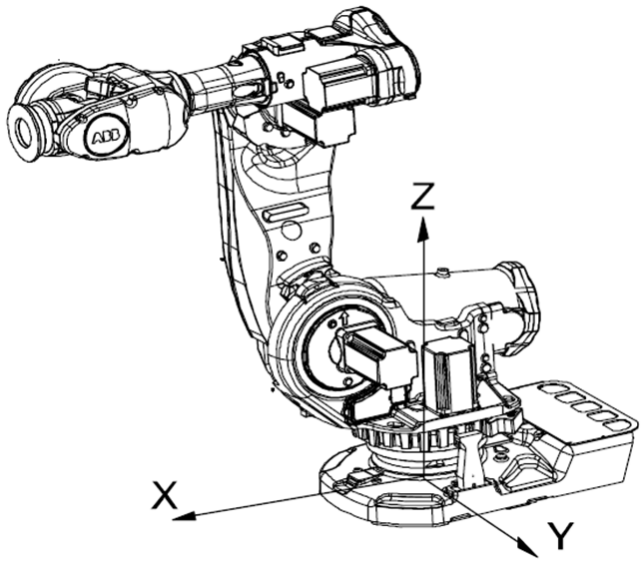

Figure 3.6: The base frame of the ABB IRB 6600 [44].

Since the second and third joints of the robot are parallel, Hayati parameter [22] is also included to the model and this parameter is calibrated instead of d_3. Following the frame assignments, the modified Denavit-Hartenberg parameters and the Hayati parameter of the robot are determined as shown in Table 3.2.

Table 3.2: Nominal Denavit-Hartenberg and Hayati parameters of the ABB IRB 6600 robot.

Link	a_i (mm)	d_i (mm)	α_i (rad)	θ_i (rad)	β_i (rad)
0	-	0	-	0	-
1	0	780	0	θ_1	-
2	320	0	$-\frac{\pi}{2}$	$\theta_2-\frac{\pi}{2}$	-
3	1075	0	0	θ_3	0
4	200	1142	$-\frac{\pi}{2}$	θ_4	-
5	0	0	$\frac{\pi}{2}$	θ_5	-
6	0	200	$-\frac{\pi}{2}$	θ_6	-
L	0	105.65	0	$-\frac{\pi}{2}$	-

3.2.3 Forward Kinematics of ABB IRB 6600

Using Eq. 3.9 and 3.10 together with the Table 3.2, the transformation from the reference frame to the end-effector frame of the robot can be calculated as:

$$ {}^{R}T_{L} = {}^{R}T_{0}\,{}^{0}T_{1}\,{}^{1}T_{2}\,{}^{2}T_{3}\,{}^{3}T_{4}\,{}^{4}T_{5}\,{}^{5}T_{6}\,{}^{6}T_{L} = \begin{bmatrix} {}^{R}R_{L} & {}^{R}P_{L} \\ 0 & 1 \end{bmatrix} \tag{3.18} $$

where ${}^{R}R_{L}$ is the 3x3 rotation matrix and ${}^{R}P_{L}$ is the 3x1 position vector.

3.2.4 Inverse Kinematics of ABB IRB 6600

The closed-form solution of the inverse kinematic model is developed algebraically using the derivations from Khalil and Dombre [6]. Only the non-zero link offsets and link lengths of the Table 3.2 are taken into consideration along with the joint angles. It can be seen from Figure 3.5 that the fourth, fifth and sixth joint axes intersect forming a spherical wrist. The origins of these frames are located at the same position making ${}^{0}P_{6} = {}^{0}P_{4}$. This can be represented by:

$$ \begin{bmatrix} p_x \\ p_y \\ p_z \\ 1 \end{bmatrix} = {}^{0}T_{1}\,{}^{1}T_{2}\,{}^{2}T_{3}\,{}^{3}T_{4} \begin{bmatrix} 0 \\ 0 \\ 0 \\ 1 \end{bmatrix} \tag{3.19} $$

Multiplying Eq. 3.19 by ${}^{2}T_{0}$ on both sides yields:

$$ \begin{bmatrix} d_1 sin\theta_2 - a_2 cos\theta_2 - p_z sin\theta_2 + p_x cos\theta_1 cos\theta_2 + p_y cos\theta_2 sin\theta_1 \\ d_1 cos\theta_2 - p_z cos\theta_2 + a_2 sin\theta_2 - p_x cos\theta_1 sin\theta_2 - p_y sin\theta_1 sin\theta_2 \\ p_y cos\theta_1 - p_x sin\theta_1 \\ 1 \end{bmatrix} = \begin{bmatrix} a_3 + a_4 cos\theta_3 - d_4 sin\theta_3 \\ d_4 cos\theta_3 + a_4 sin\theta_3 \\ 0 \\ 1 \end{bmatrix} \tag{3.20} $$

The three equations from Eq. 3.20 can be written as:

$$ a_4 cos\theta_3 - d_4 sin\theta_3 = (d_1 - p_z) sin\theta_2 - (a_2 - p_x cos\theta_1 - p_y sin\theta_1) cos\theta_2 - a_3 \tag{3.21} $$

$$ a_4 sin\theta_3 + d_4 cos\theta_3 = (d_1 - p_z) cos\theta_2 + (a_2 - p_x cos\theta_1 - p_y sin\theta_1) sin\theta_2 \tag{3.22} $$

$$ p_y cos\theta_1 - p_x sin\theta_1 = 0 \tag{3.23} $$

Eq. 3.23 can be used to solve for θ_1 as [6]:

$$\left\{ \begin{array}{l} \theta_1 = atan2(p_y, p_x) \\ \theta_1' = \theta_1 + \pi \end{array} \right\} \tag{3.24}$$

Eq. 3.22 and Eq. 3.21 can be written as:

$$W_1 cos\theta_3 + W_2 sin\theta_3 = X sin\theta_2 + Y cos\theta_2 + Z_1 \tag{3.25}$$

$$W_1 sin\theta_3 - W_2 cos\theta_3 = X cos\theta_2 - Y sin\theta_2 + Z_2 \tag{3.26}$$

where

$$\left\{ \begin{array}{l} W_1 = a_4 \\ W_2 = d_4 \\ X = d_1 - p_z \\ Y = a_2 - p_x cos\theta_1 - p_y sin\theta_1 \\ Z_1 = 0 \\ Z_2 = -a_3 \end{array} \right\} \tag{3.27}$$

Squaring and adding the both sides of the Eq. 3.22 and 3.21 cancels the terms with θ_3 and yields an equation containing only θ_2 in the form:

$$B_1 sin\theta_2 + B_2 cos\theta_2 = B_3 \tag{3.28}$$

where

$$\left\{ \begin{array}{l} B_1 = -2a_3(d_1 - p_z) \\ B_2 = 2a_3(a_2 - p_x cos\theta_1 - p_y sin\theta_1) \\ B_3 = a_4^2 - (d_1 - p_z)^2 - (a_2 - p_x cos\theta_1 - p_y sin\theta_1)^2 - a_3^2 \end{array} \right\} \tag{3.29}$$

From Eq. 3.28 [6]:

$$sin\theta_2 = \frac{B_1 B_3 + \epsilon B_2 \sqrt[2]{B_1^2 + B_2^2 - B_3^2}}{B_1^2 + B_2^2} \tag{3.30}$$

$$cos\theta_2 = \frac{B_2 B_3 - \epsilon B_1 \sqrt[2]{B_1^2 + B_2^2 - B_3^2}}{B_1^2 + B_2^2} \tag{3.31}$$

where ϵ=±1. Thus θ_2 can be solved by using Eq. 3.30 and 3.31 as:

$$\theta_2 = atan2(sin\theta_2, cos\theta_2) \tag{3.32}$$

Having found θ_2, Eq. 3.22 and 3.21 reduce to the form:

$$X_1 sin\theta_3 + Y_1 cos\theta_3 = Q_1 \tag{3.33}$$

$$X_2 sin\theta_3 + Y_2 cos\theta_3 = Q_2 \tag{3.34}$$

where

$$\left\{\begin{array}{l} X_1 = Y_2 = a_4 \\ X_2 = -Y_1 = -d_4 \\ Q_1 = (d_1 - p_z)cos\theta_2 + (a_2 - p_x cos\theta_1 - p_y sin\theta_1)sin\theta_2 \\ Q_2 = (d_1 - p_z)sin\theta_2 - (a_2 - p_x cos\theta_1 - p_y sin\theta_1)cos\theta_2 - a_3 \end{array}\right\} \tag{3.35}$$

Multiplying the Eq. 3.33 by Y_2 and 3.34 by Y_1 and adding both sides yields [6]:

$$sin\theta_3 = \frac{Q_1 Y_2 - Q_2 Y_1}{X_1 Y_2 - X_2 Y_1} \tag{3.36}$$

Multiplying the Eq. 3.33 by X_2 and 3.34 by X_1 and adding both sides yields [6]:

$$cos\theta_3 = \frac{Q_2 X_1 - Q_1 X_2}{X_1 Y_2 - X_2 Y_1} \tag{3.37}$$

Thus θ_3 can be solved by using Eq. 3.36 and 3.37 as:

$$\theta_3 = atan2(sin\theta_3, cos\theta_3) \tag{3.38}$$

After finding θ_1, θ_2 and θ_3, the rotation matrix of the third frame relative to the base frame, ${}^0R_3$, can be calculated. The rotation matrix of the final frame relative to the base frame is also known and can be written as:

$${}^0R_6 = \begin{bmatrix} s_x & n_x & a_x \\ s_y & n_y & a_y \\ s_z & n_z & a_z \end{bmatrix} \tag{3.39}$$

Thus the rotation matrix ${}^3R_6$ can be calculated from:

$${}^3R_6 = {}^3R_0\,{}^0R_6 = \begin{bmatrix} f_x & g_x & h_x \\ f_y & g_y & h_y \\ f_z & g_z & h_z \end{bmatrix} = {}^3R_0 \begin{bmatrix} s_x & n_x & a_x \\ s_y & n_y & a_y \\ s_z & n_z & a_z \end{bmatrix} \tag{3.40}$$

The same way, calculating ${}^4R_6$:

$${}^4R_6 = {}^4R_3\,{}^3R_6 = \begin{bmatrix} f_x cos\theta_4 - f_z sin\theta_4 & g_x cos\theta_4 - g_z sin\theta_4 & h_x cos\theta_4 - h_z sin\theta_4 \\ -f_z cos\theta_4 - f_x sin\theta_4 & -g_z cos\theta_4 - g_x sin\theta_4 & -h_z cos\theta_4 - h_x sin\theta_4 \\ f_y & g_y & h_y \end{bmatrix}$$

$$= \begin{bmatrix} cos\theta_5 cos\theta_6 & -cos\theta_5 - sin\theta_6 & -sin\theta_5 \\ sin\theta_6 & cos\theta_6 & 0 \\ cos\theta_6 sin\theta_5 & -sin\theta_5 sin\theta_6 & cos\theta_5 \end{bmatrix} \tag{3.41}$$

From the second rows and third columns of both sides of Eq. 3.41:

$$-h_z cos\theta_4 - h_x sin\theta_4 = 0 \tag{3.42}$$

Eq. 3.42 can be used to solve for θ_4 as [6]:

$$\left\{ \begin{array}{l} \theta_4 = atan2(h_z, -h_x) \\ \theta_4' = \theta_1 + \pi \end{array} \right\} \tag{3.43}$$

Again from Eq. 3.41:

$$sin\theta_5 = -h_x cos\theta_4 + h_z sin\theta_4 \tag{3.44}$$

$$cos\theta_5 = h_y \tag{3.45}$$

Solving Eq. 3.44 and 3.45 together for θ_5 [6]:

$$\theta_5 = atan2(sin\theta_5, cos\theta_5) \tag{3.46}$$

And lastly from Eq. 3.41:

$$sin\theta_6 = -f_z cos\theta_4 - f_x sin\theta_4 \tag{3.47}$$

$$cos\theta_6 = -g_z cos\theta_4 - g_x sin\theta_4 \tag{3.48}$$

Solving Eq. 3.47 and 3.48 together for θ_6 [6]:

$$\theta_6 = atan2(sin\theta_6, cos\theta_6) \tag{3.49}$$

CHAPTER 4

PARAMETER IDENTIFICATION

This chapter gives information about the pose selection and the parameter identification methods used during the study by their formulation, analysis and utilization to the model developed on the previous chapter.

4.1 Parameter Identification Methods

Parameter identification methods used on the previous robot calibration studies are discussed on the second chapter. Two of these algorithms based on least squares are presented in this section.

4.1.1 Gauss-Newton Algorithm

The nonlinear kinematic model can be written as [30, 31]:

$$\mathbf{y} = \mathbf{f}(\mathbf{w}, \mathbf{x}) \tag{4.1}$$

where $\mathbf{w}$ is the p x 1 parameter vector to be identified, $\mathbf{y}$ is the n x 1 output vector, $\mathbf{f}(\mathbf{w}, \mathbf{x})$ is n x 1 vector of functions and $\mathbf{x}$ is the k x 1 input vector. When there are m measurements having n pose components, Eq. 4.1 can be written as [31, 30]:

$$\mathbf{y}^{\mathrm{j}} = \mathbf{f}^{\mathrm{j}}(\mathbf{w}, \mathbf{x}^{\mathrm{j}}) \; (j = 1, \ldots, m) \tag{4.2}$$

where $\mathbf{f}^{\mathrm{j}}(\mathbf{w}, \mathbf{x}^{\mathrm{j}}) = [f_1^{\mathrm{j}}(\mathbf{w}, \mathbf{x}^{\mathrm{j}}) \ldots f_{\mathrm{n}}^{\mathrm{j}}(\mathbf{w}, \mathbf{x}^{\mathrm{j}})]^{\mathrm{T}}$ is the n x 1 vector of functions, $\mathbf{y}^{\mathrm{j}} = [y_1^{\mathrm{j}} \ldots y_{\mathrm{n}}^{\mathrm{j}}]^{\mathrm{T}}$ is the n x 1 output vector and $\mathbf{x}^{\mathrm{j}} = [x_1^{\mathrm{j}} \ldots x_{\mathrm{k}}^{\mathrm{j}}]^{\mathrm{T}}$ is the k x 1 input vector for the jth measurement.

The least-square solution seeks the estimate $\hat{\mathbf{w}}$ of the actual value of the parameter vector $\mathbf{w}$ that minimizes the sum of squares of the error between the model and the measurements:

$$S(\mathbf{w}) = \sum_{j=1}^{m} \| \mathbf{y}^{\mathrm{j}} - \mathbf{f}(\mathbf{w}, \mathbf{x}^{\mathrm{j}}) \|^2 = \mathbf{r}^{\mathrm{T}}\mathbf{r} \tag{4.3}$$

where $\mathbf{r}$ is the nm x 1 residual vector:

$$\mathbf{r} = \begin{bmatrix} y_1^1 - f_1^1(\mathbf{w}, \mathbf{x}^1) \\ y_2^1 - f_2^1(\mathbf{w}, \mathbf{x}^1) \\ \vdots \\ y_{\mathrm{n}}^{\mathrm{j}} - f_{\mathrm{n}}^{\mathrm{j}}(\mathbf{w}, \mathbf{x}^{\mathrm{j}}) \\ \vdots \\ y_{\mathrm{n-1}}^{\mathrm{m}} - f_{\mathrm{n-1}}^{\mathrm{m}}(\mathbf{w}, \mathbf{x}^{\mathrm{m}}) \\ y_{\mathrm{n}}^{\mathrm{m}} - f_{\mathrm{n}}^{\mathrm{m}}(\mathbf{w}, \mathbf{x}^{\mathrm{m}}) \end{bmatrix} \tag{4.4}$$

Taking linear Taylor series approximation of $\mathbf{f}^{\mathrm{j}}(\mathbf{w}, \mathbf{x}^{\mathrm{j}})$ about an initial estimate of the parameter vector $\mathbf{w}^{\mathrm{a}}$ yields:

$$\mathbf{f}^{\mathrm{j}}(\mathbf{w}, \mathbf{x}^{\mathrm{j}}) \approx \mathbf{f}^{\mathrm{j}}(\mathbf{w}^{\mathrm{a}}, \mathbf{x}^{\mathrm{j}}) + \frac{\partial \mathbf{f}^{\mathrm{j}}(\mathbf{w}, \mathbf{x}^{\mathrm{j}})}{\partial \mathbf{w}} |_{\mathrm{w=w^a}} (\mathbf{w} - \mathbf{w}^{\mathrm{a}}) \tag{4.5}$$

Solving for the minimum of Eq. 4.3 with respect to w using Eq. 4.5 yields [30]:

$$(\mathbf{w} - \mathbf{w}^{\mathrm{a}}) = \boldsymbol{\delta}^{\mathrm{a}} = (\mathbf{J}^{\mathrm{aT}}\mathbf{J}^{\mathrm{a}})^{-1}\mathbf{J}^{\mathrm{aT}}\mathbf{r} \tag{4.6}$$

where

$$\mathbf{J}^{\mathrm{a}} = \begin{bmatrix} \frac{\partial \mathbf{f}^1(\mathbf{w}, \mathbf{x}^1)}{\partial \mathbf{w}} |_{\mathrm{w=w^a}} \\ \vdots \\ \frac{\partial \mathbf{f}^{\mathrm{m}}(\mathbf{w}, \mathbf{x}^{\mathrm{m}})}{\partial \mathbf{w}} |_{\mathrm{w=w^a}} \end{bmatrix} \tag{4.7}$$

is the nm x p identification Jacobian matrix. Eq. 4.29 is called Gauss-Newton step [30]. Thus, given an initial estimate $\mathbf{w}^{\mathrm{a}}$, the next estimate can be calculated from:

$$\mathbf{w}^{\mathrm{a+1}} = \mathbf{w}^{\mathrm{a}} + \boldsymbol{\delta}^{\mathrm{a}} = \mathbf{w}^{\mathrm{a}} + (\mathbf{J}^{\mathrm{aT}}\mathbf{J}^{\mathrm{a}})^{-1}\mathbf{J}^{\mathrm{aT}}\mathbf{r} \tag{4.8}$$

which is repeated iteratively until the error is less than a tolerance value or a convergence is obtained.

4.1.2 Levenberg - Marquardt Algorithm

Gauss-Newton algorithm is known for its fast convergence. However, a problem arise when the matrix $\mathbf{J}^{\mathrm{T}}\mathbf{J}$ is not invertible for being singular or ill-conditioned. Levenberg and Marquardt

algorithm solves this problem by modifying the Gauss-Newton step as [30, 32, 33]:

$$\boldsymbol{\delta}^{a} = (\mathbf{J}^{aT}\mathbf{J}^{a} + \mu^{a}\mathbf{D}^{a})^{-1}\mathbf{J}^{aT}\mathbf{r} \tag{4.9}$$

where $\mathbf{D}^{a}$ is a diagonal matrix containing positive elements and $\mu^{a}$is a scalar. $\mathbf{D}^{a}$ can be chosen as identity matrix for simplicity or the diagonal elements of the matrix $\mathbf{J}^{aT}\mathbf{J}^{a}$ are used. μ^{a} is generally set as a low value and it is multiplied by a factor whenever Eq. 4.3 is not reduced as a result of the iteration.

4.2 Parameter Identification of ABB IRB 6600

In this section, the details of the employment of the parameter identification procedure for ABB IRB 6600 robot are presented.

4.2.1 Formulation

For the utilized robot calibration scheme and according to Eq 4.2 and 4.8, output vector consists of the pose measurements, input vector consists of the joint variables and the parameters not included on the identification and the vector of functions are the nonlinear equations obtained from Eq 3.18.

The parameter vector is a 30 x 1 vector consisting of all 30 parameters of Table 3.2:

$$\mathbf{w} = [\alpha_1 \ldots \alpha_L \; a_1 \ldots a_L \; d_0 \ldots d_2 \; d_4 \ldots d_L \; \theta_0 \ldots \theta_L \; \beta_3]^T \tag{4.10}$$

with the assumption of all parameters being identifiable. The identifiability of the parameters will be investigated on the next section.

Let m pose measurements be taken from the robot's end-effector frame having three position and three orientation components. The joint configurations of the robot corresponding to the jth measurement can be expressed as :

$$\boldsymbol{\theta}^{j} = [\theta^{j}_{1,meas} \; \theta^{j}_{2,meas} \; \theta^{j}_{3,meas} \; \theta^{j}_{4,meas} \; \theta^{j}_{5,meas} \; \theta^{j}_{6,meas}]^T \quad (j = 1, \ldots, m) \tag{4.11}$$

and the jth measurement can be expressed as:

$$\mathbf{y}^{j} = [P^{j}_{x,meas} \; P^{j}_{y,meas} \; P^{j}_{z,meas} \; \gamma^{j}_{x,meas} \; \gamma^{j}_{y,meas} \; \gamma^{j}_{z,meas}]^T \quad (j = 1, \ldots, m) \tag{4.12}$$

where the superscript 'meas' denotes that these are obtained from measurements. Same way, the pose of the end-effector for the jth measurement configuration can be calculated using Eq. 3.18 and 4.11 together with the parameters from Table 3.2 as:

$$ {}^{R}T_{L,calc} = \begin{bmatrix} {}^{R}\mathbf{R}^{j}_{L,calc} & \begin{matrix} P^{j}_{x,calc} \\ P^{j}_{y,calc} \\ P^{j}_{z,calc} \end{matrix} \\ \mathbf{0} & 1 \end{bmatrix} \; (j = 1, \ldots, m) \tag{4.13} $$

where the superscript 'calc' denotes that these are obtained from calculations. In order to form the residue vector for the jth measurement configuration, the difference between the calculated and the measured position and orientation of the end-effector is needed to be obtained:

$$ \mathbf{r}^{j} = \begin{bmatrix} \Delta\mathbf{P}^{j} \\ \Delta\mathbf{O}^{j} \end{bmatrix} \; (j = 1, \ldots, m) \tag{4.14} $$

Since the measurement system represents the orientation using Z-Y-X Euler angles, the Euler angles from the matrix ${}^{R}\mathbf{R}^{c}_{L,calc}$ can be extracted. However, the calculation of the identification Jacobian will be far too tedious using this approach. For this reason, the approach of Khalil and Dombre is used to represent the orientation error by using rotation matrices. The rotation matrix from the jth measured orientation can be calculated by:

$$ {}^{R}\mathbf{R}^{j}_{L,meas} = Rot(z, \gamma^{j}_{z,meas}) Rot(y, \gamma^{j}_{y,meas}) Rot(x, \gamma^{j}_{x,meas}) \tag{4.15} $$

and the orientation error can be expressed as [6]:

$$ \Delta\mathbf{O}^{j} = \mathbf{u}^{j}\alpha^{j} \tag{4.16} $$

where

$$ {}^{R}\mathbf{R}^{j}_{L,meas} = Rot(\mathbf{u}^{j}, \alpha^{j}) {}^{R}\mathbf{R}^{j}_{L,calc} \tag{4.17} $$

Thus, the 6m x 1 residue vector becomes:

$$\mathbf{r} = \begin{bmatrix} \mathbf{r}_1 \\ \mathbf{r}^2 \\ \vdots \\ \mathbf{r}^{\mathrm{m}} \end{bmatrix} = \begin{bmatrix} \Delta\mathbf{P}^1 \\ \Delta\mathbf{O}^1 \\ \vdots \\ \Delta\mathbf{P}^{\mathrm{m}} \\ \Delta\mathbf{O}^{\mathrm{m}} \end{bmatrix} = \begin{bmatrix} P^1_{\mathrm{x,meas}} - P^1_{\mathrm{x,calc}} \\ P^1_{\mathrm{y,meas}} - P^1_{\mathrm{y,calc}} \\ P^1_{\mathrm{z,meas}} - P^1_{\mathrm{z,calc}} \\ u^1_1\alpha^1 \\ u^1_2\alpha^1 \\ u^1_3\alpha^1 \\ \vdots \\ P^{\mathrm{m}}_{\mathrm{x,meas}} - P^{\mathrm{m}}_{\mathrm{x,calc}} \\ P^{\mathrm{m}}_{\mathrm{y,meas}} - P^{\mathrm{m}}_{\mathrm{y,calc}} \\ P^{\mathrm{m}}_{\mathrm{z,meas}} - P^{\mathrm{m}}_{\mathrm{z,calc}} \\ u^{\mathrm{m}}_1\alpha^{\mathrm{m}} \\ u^{\mathrm{m}}_2\alpha^{\mathrm{m}} \\ u^{\mathrm{m}}_3\alpha^{\mathrm{m}} \end{bmatrix} \tag{4.18}$$

For pose measurements, the identification Jacobian has one row for each of the six pose element of each of the m measurements and one column for each of the p parameters making it a 6m x p matrix. The individual Jacobian matrices of the parameters can be calculated by [6, 31]:

$$\mathbf{J}^{\mathrm{j}}_{\alpha_{\mathrm{i}}} = \begin{bmatrix} {}^{\mathrm{R}}\mathbf{x}^{\mathrm{j}}_{\mathrm{i-1}} \times {}^{\mathrm{R}}\mathbf{d}^{\mathrm{j}}_{\mathrm{i-1,L}} \\ {}^{\mathrm{R}}\mathbf{x}^{\mathrm{j}}_{\mathrm{i-1}} \end{bmatrix} \tag{4.19}$$

$$\mathbf{J}^{\mathrm{j}}_{\mathrm{a}_{\mathrm{i}}} = \begin{bmatrix} {}^{\mathrm{R}}\mathbf{x}^{\mathrm{j}}_{\mathrm{i-1}} \\ 0 \end{bmatrix} \tag{4.20}$$

$$\mathbf{J}^{\mathrm{j}}_{\mathrm{d}_{\mathrm{i}}} = \begin{bmatrix} {}^{\mathrm{R}}\mathbf{z}^{\mathrm{j}}_{\mathrm{i}} \\ 0 \end{bmatrix} \tag{4.21}$$

$$\mathbf{J}^{\mathrm{j}}_{\theta_{\mathrm{i}}} = \begin{bmatrix} {}^{\mathrm{R}}\mathbf{z}^{\mathrm{j}}_{\mathrm{i}} \times {}^{\mathrm{R}}\mathbf{d}^{\mathrm{j}}_{\mathrm{i,L}} \\ {}^{\mathrm{R}}\mathbf{z}^{\mathrm{j}}_{\mathrm{i}} \end{bmatrix} \tag{4.22}$$

$$\mathbf{J}^{j}_{\beta_i} = \begin{bmatrix} {}^{R}\mathbf{y}^{j}_{i-1} \times {}^{R}\mathbf{d}^{j}_{i-1,L} \\ {}^{R}\mathbf{y}^{j}_{i-1} \end{bmatrix} \; (j = 1, \ldots, m) \tag{4.23}$$

for $(j = 1, \ldots, m)$ where

$$ {}^{R}\mathbf{d}^{j}_{i,L} = {}^{R}\mathbf{R}^{j}_{i}\, {}^{i}\mathbf{P}^{j}_{L} \tag{4.24}$$

is the vector connecting the origin of the coordinate frame i to the origin of the coordinate frame L [6, 31]. Concatenating all individual Jacobian matrices for all p parameters for the jth measurement yields 6 x p matrix:

$$\mathbf{J}^{j} = [\mathbf{J}^{j}_{\alpha_1} \ldots \mathbf{J}^{j}_{\alpha_L}\; \mathbf{J}^{j}_{a_1} \ldots \mathbf{J}^{j}_{a_L}\; \mathbf{J}^{j}_{d_0} \ldots \mathbf{J}^{j}_{d_2} \mathbf{J}^{j}_{d_4} \ldots \mathbf{J}^{j}_{d_L}\; \mathbf{J}^{j}_{\theta_0} \ldots \mathbf{J}^{j}_{\theta_L}\; \mathbf{J}^{j}_{\beta_3}] \tag{4.25}$$

and concatenating this matrix for all m measurements yields the 6m x p generalized Jacobian matrix:

$$\mathbf{J} = \begin{bmatrix} \mathbf{J}^{1} \\ \mathbf{J}^{2} \\ \vdots \\ \mathbf{J}^{m} \end{bmatrix} \tag{4.26}$$

4.2.2 Identifiability

It is known that some parameters of the model cannot be identified as a result of zero or linearly dependent columns of the matrix **J**. If a column of the matrix **J** is zero, then the parameter corresponding to that column has no effect on the output and thus cannot be identified. Furthermore, the rank of the matrix **J** equals to the number of parameters that can be identified [6].

The parameters of the robot that are not identifiable can be obtained using the method presented by Khalil et.al [29]. According to this, the identifiable parameters of the robot are determined using a QR decomposition of **J** as [29]:

$$\mathbf{J} = \mathbf{Q} \begin{bmatrix} \mathbf{R} \\ \mathbf{0}_{(r-c)xc} \end{bmatrix} \tag{4.27}$$

where Q is an r x r orthogonal matrix, R is a c x c upper triangular matrix and 0 is a (r-c) x c zero matrix [29]. The non-identifiable parameters correspond to the absolute value elements

on the diagonal of the matrix R, $|\ \mathbf{R}(\mathbf{k},\mathbf{k})\ |$ $(k = 1, \ldots, r)$, that are less than a tolerance value [29]. This tolerance value can be selected as the number of rows times the computer precision [29]. It is also suggested to change the order of the columns of the matrix **J** by first placing the parameters whose values can be changed from the control system [6]. After identifying non-identifiable parameters, the corresponding columns of the matrix **J** are removed.

We have applied this method using random generated pose measurements. The results are given in Table 4.1. According to this, the parameters θ_0, d_0, θ_L and d_L cannot be identified. The reason for this can be explained as the zero valued α_1, a_1, α_L and a_L parameters make these parameters' effect to be grouped with other parameters. The effect of the parameters θ_0 and θ_L are grouped with θ_1 and θ_6 and the effect of the parameters d_0 and d_L are grouped with d_1, d_6, respectively.

Table 4.1: The identifiable and non-identifiable parameters of the ABB IRB 6600 robot. (I : identifiable parameter, N : non-identifiable parameter, - : no effect on the model)

Link	a_i	d_i	α_i	θ_i	β_i
0	-	N	-	N	-
1	I	I	I	I	-
2	I	I	I	I	-
3	I	-	I	I	I
4	I	I	I	I	-
5	I	I	I	I	-
6	I	I	I	I	-
L	I	N	I	N	-

According to Table 4.1, the parameter vector reduces to:

$$\mathbf{w} = [\alpha_1 \ldots \alpha_L\ a_1 \ldots a_L\ d_1 \ldots d_2\ d_4 \ldots d_6\ \theta_1 \ldots \theta_6\ \beta_3]^T \tag{4.28}$$

The columns of the matrix **J** corresponding to the non-identifiable parameters are removed. We will refer to the resulting matrix **J** still for simplicity.

4.2.3 Scaling

The position and the orientation components of the pose measurements have different units as millimeters and radians respectively. The accuracy of the measurement system also differs among these components. Thus, the corresponding errors corresponding cannot be compared

directly. In order to overcome this problem, Eq. 4.29 can be scaled by an appropriate weighting matrix **W** as [31]:

$$(\mathbf{w} - \mathbf{w}^{\mathrm{a}}) = \boldsymbol{\delta}^{\mathrm{a}} = (\mathbf{J}^{\mathrm{aT}}\mathbf{W}\mathbf{J}^{\mathrm{a}})^{-1}\mathbf{J}^{\mathrm{aT}}\mathbf{W}\mathbf{r} \tag{4.29}$$

The measurement system used to obtain pose measurements is capable of giving the standard deviation values of the measured variables. Let the standard deviation of the kth pose component of the jth measurement be $\sigma^{\mathrm{j}}_{\mathrm{k}}$ for $(k = 1, \ldots, 6)$ and $(j = 1, \ldots, m)$. These standard deviation values can be used on the corresponding diagonal element of the weighting matrix as [31]:

$$\mathbf{W} = \begin{bmatrix} (\frac{1}{\sigma^{1}_{1}})^2 & \ldots & \ldots & \ldots & \ldots & 0 \\ 0 & (\frac{1}{\sigma^{1}_{2}})^2 & \ldots & \ldots & \ldots & 0 \\ \vdots & & \ddots & & & \vdots \\ 0 & \ldots & \ldots & (\frac{1}{\sigma^{\mathrm{j}}_{\mathrm{k}}})^2 & \ldots & 0 \\ \vdots & & & & \ddots & \vdots \\ 0 & \ldots & \ldots & \ldots & \ldots & (\frac{1}{\sigma^{\mathrm{m}}_{6}})^2 \end{bmatrix} \quad \begin{matrix} k = 1, \ldots, 6 \\ j = 1, \ldots, m \end{matrix} \tag{4.30}$$

4.3 Pose Selection

The success of the parameter identification on finding accurate estimates of the parameters is effected by the measurement noise, the number of measurements and the selection of measurement configurations [36]. A common practice to suppress the measurement noise in order to achieve better estimates of the parameters is to increase the number of measurements used in the identification step. However, a better approach is to select the measurement configurations which will yield good estimates.

The determination of a set of reachable robot measurement configurations that minimizes the effect of the measurement noise on the identification of robot kinematic parameters is the subject of the optimal pose selection algorithms [35]. These measurement configurations are selected using an observability index based on the identification Jacobian matrix. Several observability indices are proposed to be used on robot calibration experiments which are related to the alphabet optimalities of the experimental design literature by Sun and Hollerbach [39]:

- O_1 is proposed by Borm and Menq [37]. It is the geometric mean of all the singular

values of the identification Jacobian:

$$O_1 = \frac{(\sigma_1 \sigma_2 \cdots \sigma_k)^{\frac{1}{k}}}{\sqrt{k}} \tag{4.31}$$

- Driels and Pathre proposed the condition number of the identification Jacobian as the observability index to be minimized [36]. Since all other observability indices are maximized, it is taken as the inverse of the condition number of the identification Jacobian [38]:

$$O_2 = \frac{\sigma_{Min}}{\sigma_{Max}} \tag{4.32}$$

- O_3 is proposed by Nahvi and Hollerbach [38]. It is the minimum singular value of the identification Jacobian:

$$O_3 = \sigma_{Min} \tag{4.33}$$

- O_4 is again proposed by Nahvi and Hollerbach [38]. It is the square of smallest non-zero singular value divided by the largest singular value of the identification Jacobian:

$$O_4 = \frac{\sigma_{Min}^2}{\sigma_{Max}} \tag{4.34}$$

In this study, we have selected O_1 as the observability index for its scale invariant characteristic that also corresponds to the D-optimal design of the experimental design literature [39].

A search algorithm is used to obtain the measurements configurations that maximize the selected observability index amongst a set of all possible measurement configurations. DETMAX, a popular algorithm proposed by Mitchell can be used to find the measurement configurations that maximize the observability index [41]. The basic algorithm follows the procedure below:

1. Start by choosing a set of m measurement configurations randomly from the possible candidate measurement configurations.

2. Add a new measurement configuration to the current set amongst the candidate set that makes the maximum increase in the observability index.

3. Remove the measurement configuration amongst the current set that makes the minimum decrease in the observability index.

4. Repeat 2 and 3 until the observability index does not increase.

This procedure improves the observability index of a randomly selected set by exchanging measurement configurations at each iteration. The original algorithm also performs a method called excursion that adds or removes new measurement configurations to improve the current set. A variation of the algorithm is proposed by Sun and Hollerbach which starts with a randomly selected set size, improves the set using the exchanging step then adds new measurement configurations until a predefined number is reached [42]. In this study, a variation of the DETMAX is used which first calculates the observability index of the whole candidate set and then removes the measurement configurations that makes the minimum decrease in the observability index until a pre-defined number of measurements is reached. The algorithm then uses this as the initial set and applies the DETMAX algorithm until observability index does not increase. The algorithm then removes a pose within the selected set and searches the candidate set for a better pose that increases the observability index. This algorithm follows the procedure below:

1. Start by choosing all measurement configurations of the candidate set.
2. Remove the measurement configuration amongst the current set that makes the minimum decrease in the observability index.
3. Repeat 2 until a pre-defined number of measurements is reached.
4. Add a new measurement configuration to the current set amongst the candidate set that makes the maximum increase in the observability index.
5. Remove the measurement configuration amongst the current set that makes the minimum decrease in the observability index.
6. Repeat 4 and 5 until the observability index does not increase.
7. Remove a measurement configuration amongst the current set and search for a measurement configuration on the candidate set that further increases the observability index.
8. Repeat 7 for all measurements in the current set until the observability index does not increase.

The major advantage of the algorithm is starting with a selected initial set instead of a random one. The concatenated identification Jacobian in Eq. 4.26 is calculated only once in the first step. It should be noted that as the number of measurements in the candidate set increases, the calculation of the identification Jacobian for all candidate measurements will require more computer time. However, it takes less than three minutes in Matlab by using a PC with Intel 2.4 GHz processor and 3 GBs of RAM for a candidate set of 300 measurement configurations and 24 model parameters which correspond to an 1800 x 24 matrix. This algorithm is used during the simulations and the experiments. The designed graphical interface is shown in Appendix A.

CHAPTER 5

SIMULATIONS

This chapter presents the details and the results of the simulations of the kinematic calibration procedure that is performed by using the developed code and the designed user interface in MATLAB.

5.1 Simulation Parameters

The model of ABB IRB 6600 robot previously developed in the Chapter 3 is used during the simulations. The actual values of the parameters to be identified are generated by adding pre-defined deviations to the nominal parameters of this robot given in Table 3.2. The deviations from the nominal parameters are shown in Table 5.1. These deviations are selected to characterize the identified deviations in previous calibration experiments.

Table 5.1: Selected deviations from the nominal Denavit - Hartenberg and Hayati parameters for simulations.

Link	a_i (mm)	d_i (mm)	α_i (mrad)	θ_i (mrad)	β_i (mrad)
0	-	-	-	-	-
1	1.4	2.1	1.8	0.9	-
2	-0.6	0.4	-0.7	-3.8	-
3	0.4	-	1.2	1.7	-0.8
4	-2.8	2.5	1.9	2.9	-
5	-0.9	-1.8	-1.6	-4.8	-
6	0.7	0.9	1.4	3.9	-
L	-0.4	-	0.9	-	-

5.2 Simulation Measurements

In order to obtain the measurement configurations to be used during the simulations, random joint angle configurations are generated. These joint values are then used to solve the end-effector pose using Eq 3.18. A sample measurement sensor is assigned to a selected location to illustrate the conditions to be faced during the experiments. Each generated measurement is checked inside the code to verify if:

- the joint angle values are inside the range of movement of the robot joints shown in Table 3.1.

- the z-axis of the robot end-effector frame inclines towards the sample measurement sensor by an angle of less than 30°.

The need for the first condition is self evident while the second condition is commonly sought by different measurement systems [46]. A total of 300 pose measurements are generated with these specifications.

Three different measurement noise settings are selected typifying different measurement system specifications from low measurement noise to high measurement noise. The measurement noise settings N1 and N3 are toward the both ends of the typical accuracy specifications of the current measurement systems while N2 is in between. The corresponding specifications are shown in Table 5.2. A normally distributed noise is added to the generated measurements with zero mean and a standard deviation value corresponding to each setting.

Table 5.2: Three measurement noise settings used during the simulations. Values represent the standard deviation values.

Measurement Noise Setting	Position Errors (mm)	Orientation Errors (mrad)
N1	0.050	0.250
N2	0.250	1.000
N3	1.000	10.000

5.3 Simulation Results

Amongst the generated 300 measurements, a set of 30 pose measurements are selected using the pose selection algorithm discussed in Section 4.3 with random deviations from the nominal parameters. Additionally, 100 pose sets of 30 measurements are selected randomly. Simulations are performed using the three different measurement noise settings.

Table 5.3: The estimation errors on the parameters after the identification with the selected and 100 random measurement poses for N1 measurement noise settings.

Parameter	Selected Set	100 Random Sets			
		Mean	Std Dev	Maximum	Minimum
α_1 (mrad)	0.0016	0.0080	0.0058	0.0270	0.0002
α_2 (mrad)	0.0345	0.0170	0.0141	0.0558	0.0001
α_3 (mrad)	0.0142	0.0149	0.0110	0.0556	0.0003
α_4 (mrad)	0.0796	0.0526	0.0408	0.1913	0.0002
α_5 (mrad)	0.0338	0.0428	0.0347	0.1450	0.0004
α_6 (mrad)	0.0389	0.0612	0.0534	0.2737	0.0010
α_7 (mrad)	0.0410	0.0578	0.0456	0.2283	0.0002
a_1 (μm)	23.5508	15.6856	12.7318	66.9892	0.2029
a_2 (μm)	4.9088	13.6028	11.0028	60.1883	0.2190
a_3 (μm)	8.8517	16.9422	12.0693	51.0957	0.1696
a_4 (μm)	28.8407	57.7177	40.2227	205.2924	0.3722
a_5 (μm)	9.5533	8.2622	6.4702	34.5722	0.0267
a_6 (μm)	8.8604	25.7720	17.2785	74.027	0.0626
a_7 (μm)	2.3841	9.1991	7.6838	39.7336	0.1072
d_1 (μm)	0.7375	19.5358	14.1109	66.4082	0.2172
d_2 (μm)	111.0884	72.9885	55.9308	296.7127	0.3825
d_4 (μm)	2.4915	13.9625	11.4551	46.345	0.0665
d_5 (μm)	1.5375	22.3674	15.4093	81.2006	0.0169
d_6 (μm)	5.6842	15.4013	11.5797	45.8911	0.0813
β_3 (mrad)	0.0060	0.0231	0.0183	0.1049	0.0001
θ_1 (mrad)	0.0086	0.0118	0.0078	0.0338	0.0002
θ_2 (mrad)	0.0015	0.0118	0.0093	0.0517	0.0001
θ_3 (mrad)	0.0012	0.0467	0.0332	0.1757	0.0002
θ_4 (mrad)	0.0546	0.0526	0.0437	0.2076	0.0011
θ_5 (mrad)	0.0458	0.0807	0.0576	0.2131	0.0014
θ_6 (mrad)	0.0102	0.0584	0.0457	0.1854	0.0001

The algorithm is run until the change in the sum of errors did not exceed the defined tolerance value or the algorithm reached the tenth iteration, whichever is satisfied first. It is seen that the algorithm is typically converged at the third iteration during the simulations.

The estimated parameters using the selected and the random measurement sets with the three different measurement noise settings are obtained as a result of the identification. The estimation errors of the parameters are calculated subsequently. The estimation errors as a result of using the selected measurement set and the mean, standard deviation, minimum and maximum values of the estimation errors of the 100 randomly selected measurement sets are given in Table 5.3, Table 5.4 and Table 5.5 for the measurement noise settings of N1, N2 and N3, respectively.

Table 5.4: The estimation errors on the parameters after the identification with the selected and 100 random measurement poses for N2 measurement noise settings.

Parameter	Selected Set	100 Random Sets			
		Mean	Std Dev	Maximum	Minimum
α_1 (mrad)	0.0482	0.0376	0.0300	0.1156	0.0001
α_2 (mrad)	0.1210	0.0921	0.0750	0.3875	0.0002
α_3 (mrad)	0.0581	0.0978	0.0793	0.4095	0.0029
α_4 (mrad)	0.0416	0.1451	0.1361	0.6950	0.0028
α_5 (mrad)	0.2761	0.2108	0.1539	0.7122	0.0042
α_6 (mrad)	0.2036	0.2558	0.1715	0.6900	0.0024
α_7 (mrad)	0.1585	0.1557	0.1097	0.4642	0.0011
a_1 (μm)	33.5517	70.4557	47.7130	217.7175	2.0720
a_2 (μm)	30.7549	61.9992	42.4049	185.2703	0.0770
a_3 (μm)	93.4090	69.7995	55.0532	319.4057	6.2720
a_4 (μm)	32.8806	240.1368	178.9645	929.1629	2.8228
a_5 (μm)	7.4534	44.2052	39.4055	156.6713	1.1718
a_6 (μm)	100.4832	78.6359	63.9825	267.9645	0.2904
a_7 (μm)	37.3922	40.0806	29.8593	130.3944	0.7499
d_1 (μm)	23.6798	88.7227	67.9779	297.3944	0.0147
d_2 (μm)	111.6598	221.7165	195.8795	965.3537	2.6871
d_4 (μm)	2.9440	65.3376	47.0604	220.5559	2.7517
d_5 (μm)	92.3698	84.1574	59.523	263.3939	2.6731
d_6 (μm)	38.3967	72.5987	59.8373	258.1521	0.2953
β_3 (mrad)	0.1763	0.1182	0.0858	0.3562	0.0003
θ_1 (mrad)	0.0455	0.0713	0.0481	0.2313	0.0045
θ_2 (mrad)	0.0286	0.0639	0.0488	0.2571	0.0015
θ_3 (mrad)	0.1147	0.2021	0.1611	0.7058	0.0028
θ_4 (mrad)	0.1463	0.1657	0.1084	0.5029	0.0008
θ_5 (mrad)	0.0659	0.2149	0.1566	0.6085	0.0040
θ_6 (mrad)	0.3563	0.1805	0.1265	0.4957	0.0013

According to the results, the estimation errors of the majority of the parameters as a result of using the selected set are lower than the mean estimation errors of the random measurement

Table 5.5: The estimation errors on the parameters after the identification with the selected and 100 random measurement poses for N3 measurement noise settings.

Parameter	Selected Set	100 Random Sets			
		Mean	Std Dev	Maximum	Minimum
α_1 (mrad)	0.1122	0.1416	0.1087	0.5548	0.0029
α_2 (mrad)	0.0641	0.2477	0.2252	1.1814	0.0005
α_3 (mrad)	0.3040	0.2887	0.2401	1.0702	0.0027
α_4 (mrad)	0.4693	1.1215	0.7828	4.0159	0.0269
α_5 (mrad)	0.3904	1.5373	1.1591	5.0538	0.0036
α_6 (mrad)	1.4286	2.0433	1.5079	7.0607	0.0113
α_7 (mrad)	1.3107	1.7109	1.1212	5.3871	0.0341
a_1 (μm)	91.9171	285.1930	224.4986	1019.3694	15.5736
a_2 (μm)	221.2678	257.4095	183.572	948.7224	0.3379
a_3 (μm)	72.0038	318.4650	247.2734	1053.8038	19.0512
a_4 (μm)	1021.4054	1682.0697	1497.8808	6874.5120	33.1173
a_5 (μm)	200.4170	202.9231	150.6137	728.0176	3.5471
a_6 (μm)	194.6515	689.2206	522.3856	2249.1379	12.2043
a_7 (μm)	240.7128	182.1121	139.9168	596.5965	9.4795
d_1 (μm)	44.0840	272.1218	226.5885	852.5135	1.6314
d_2 (μm)	614.556	1646.3328	1017.1755	4671.4076	32.5613
d_4 (μm)	90.0670	294.4104	235.2510	1105.2158	6.1125
d_5 (μm)	138.0201	688.8379	506.4906	2286.4000	16.1572
d_6 (μm)	481.0500	269.6825	216.2379	1025.7758	5.4026
β_3 (mrad)	0.2569	0.4316	0.3343	1.4242	0.0029
θ_1 (mrad)	0.0969	0.1894	0.1422	0.5986	0.0031
θ_2 (mrad)	0.0070	0.2417	0.1901	0.8544	0.0069
θ_3 (mrad)	0.9066	1.4054	1.2347	4.9963	0.0100
θ_4 (mrad)	0.5248	1.0806	0.7541	3.2314	0.0161
θ_5 (mrad)	0.0726	2.2977	1.6817	7.1829	0.0118
θ_6 (mrad)	0.6941	2.3968	2.0548	9.1961	0.0081

sets. Only the estimation errors of a_1, a_5, d_2, α_2, α_4 and θ_4 in the selected measurement set are greater than the mean estimation errors of the random measurement sets using the least measurement noise setting N1. The same way, the estimation errors of a_3, a_6, d_5, α_1, α_2, α_5, α_7, β_3 and θ_6 using N2 measurement noise setting and the estimation errors of a_7, d_6 and α_3 using N3 measurement noise setting in selected measurement set are greater than the mean estimation errors of the random measurement sets. Only the estimation errors of α_2 for the N1 measurement noise setting and θ_6 for the N2 measurement noise setting are greater than the mean plus the standard deviation value of the estimation errors of random sets.

The expected effect of the measurement noise on the estimation errors of parameters can

also be seen on these tables, in that, as the measurement noise increases, the estimation errors rapidly deteriorate. Especially, using the N3 measurement noise setting, most of the maximum estimation errors of the random sets are greater than the initial errors of the parameters.

Table 5.6: The RMS errors of the end effector pose before and after identification with optimally selected measurement poses having three different measurement noise profile.

Pose Component	Initial Error	N1	N2	N3
ΔP_X (mm)	1.367	0.010	0.048	0.158
ΔP_Y (mm)	1.238	0.011	0.043	0.175
ΔP_Z (mm)	1.897	0.009	0.040	0.135
$\Delta \gamma_X$ (mrad)	4.233	0.044	0.356	0.991
$\Delta \gamma_Y$ (mrad)	1.855	0.024	0.128	0.410
$\Delta \gamma_Z$ (mrad)	3.969	0.039	0.365	1.174

After the selected pose measurements are removed from the initial set of 300 generated pose measurements, the remaining set is used to examine the pose errors of the robot end-effector prior to and after the calibration. The results are shown in Table 5.6 for using the selected pose measurements with different measurement noise specifications.

According to the results using the lowest measurement noise settings, the initial errors are reduced for more than 98% for all pose components. For the highest measurement noise, while the improvements on robot pose accuracy significantly dropped, the initial errors are still reduced for more than 70% for all pose components. The worst effected pose components from the measurement noise are the ones representing the orientation. On the other hand, the positioning accuracy improvements from the initial errors are still higher than 85% despite this high measurement noise setting. As an expected result, it can be seen that the improvements on robot pose accuracy greatly decrease as the measurement noise further increases.

CHAPTER 6

EXPERIMENTS

This chapter presents the details and the results of the kinematic calibration experiments that are performed by using the developed code and the designed user interface in MATLAB.

6.1 Experimental Setup

The experiments are performed on an ABB IRB 6600 industrial robot. The nominal Denavit-Hartenberg and Hayati parameters of this robot are derived in the Chapter 3 which are given in Table 3.2.

6.1.1 Measurement System

Leica LTD 500 Laser Tracker is used as the measurement system during the experiments. This laser tracker system uses the absolute distance measurements together with the two angle values from the encoder readings to obtain 3D measurements. In order to obtain full pose measurements from the robot, a Leica T-Mac probe is used which is directly mounted on the robot end-effector using an apparatus as shown in Figure 6.1. The accuracy specifications of the Leica LTD500 laser tracker and the T-Mac probe are shown in Table 6.1.

In order to register the reference coordinate system to the measurement system, the reference guides on the robot body are used. There are a total of four reference guides on the robot and the center of the reference guides are on a circle with its center about on the base frame origin and having a radius of 400 mm which can be seen in Figures 6.3. Concerning the rapid

Figure 6.1: Experimental setup with Leica T-Mac mounted on the terminal frame of the robot and Leica LTD500 laser tracker.

Table 6.1: Accuracy specifications of Leica LTD 500 laser tracker and Leica T-Mac probe [45, 46].

Leica LTD500 Absolute accuracy of a coordinate for non-moving target (2σ value)	$\pm 10\mu$m/m + 6 μm/m
Leica T-Mac Accuracy of rotation angles (Maximum Permissible Error)	0.01°
Leica T-Mac Positional accuracy (Maximum Permissible Error)	$\pm 15\mu$m + 6μm/m

measurements to be taken from these reference guides, an apparatus that can be mounted inside the reference guide holes is designed according to the dimensions of the reference guide holes shown in Figure 6.4. The apparatus is also designed so that 1.5' reflectors can be placed on top of it as seen on the Figure 6.2. The calculated positions of the center of these reference guides are shown in Table 6.2. Figure 6.5 shows one of the reference guides, the designed apparatus placed on it and the reflector placed on top of the apparatus.

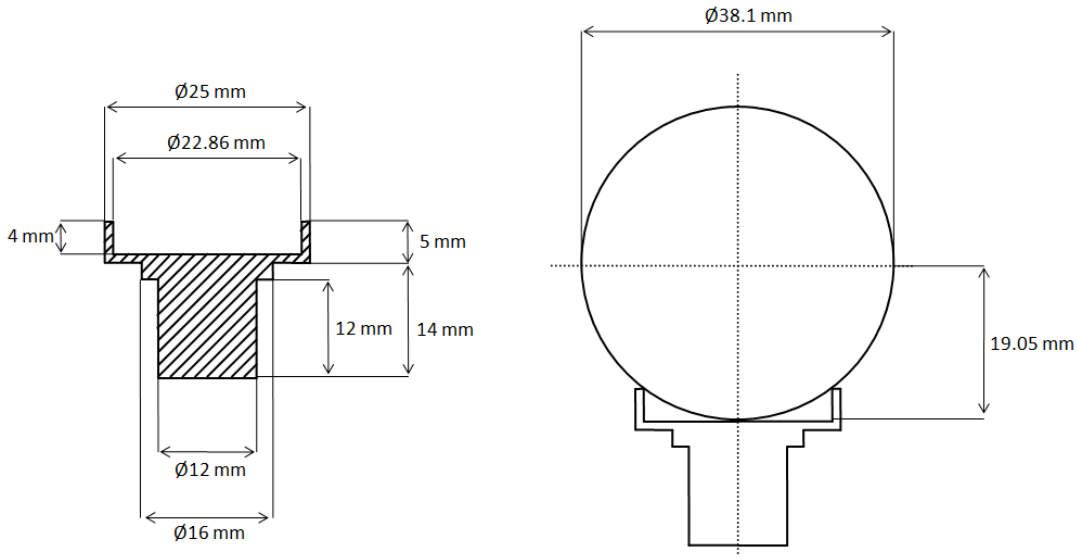

Figure 6.2: The technical drawings of the designed apparatus for the reference guide holes and the 1.5” reflectors’ position on top of it.

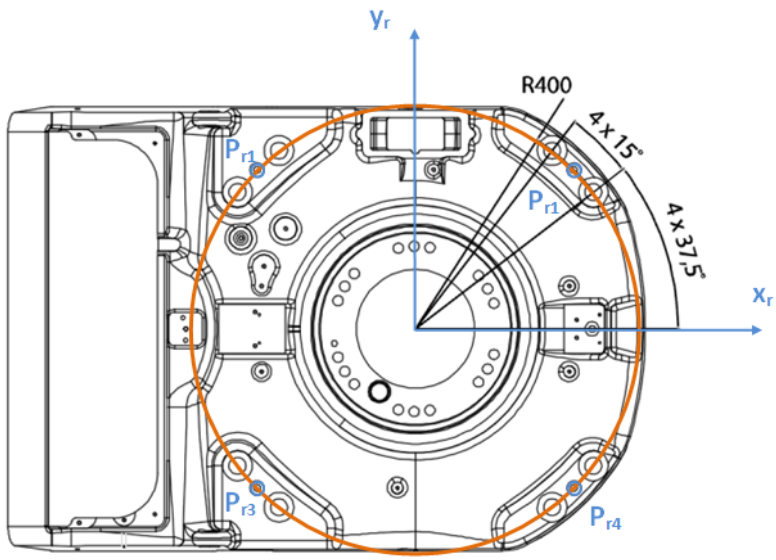

Figure 6.3: The top view of the four reference guides of the robot [44]. Dimensions are in mm and radian.

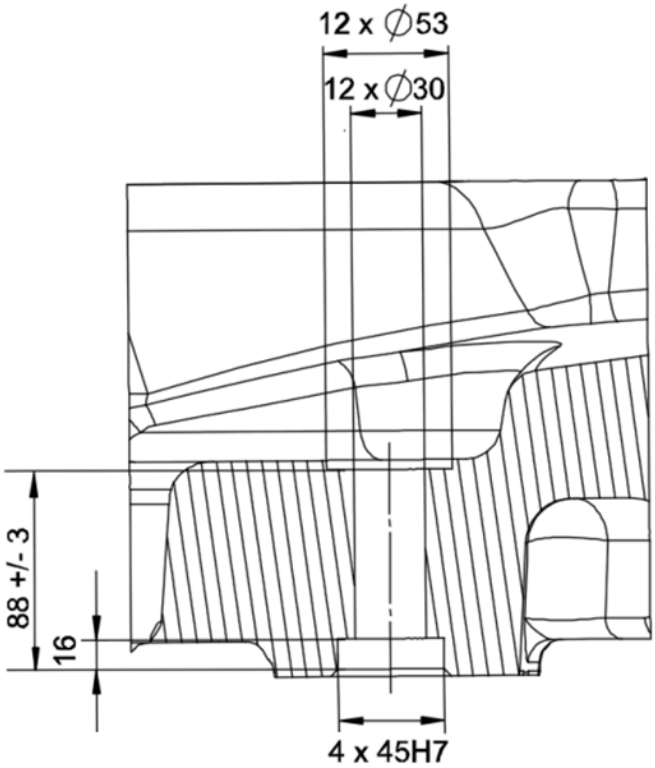

Figure 6.4: The side-view of the reference guides of the robot [44]. Dimensions are in mm.

(a) (b) (c)

Figure 6.5: The images showing (a) reference guide, (b) the placing of the designed apparatus to the reference guide and (c) the reflector placed on top of the apparatus facing the measurement system sensor.

Table 6.2: The position of the four reference guides.

Point	X (mm)	Y (mm)	Z (mm)
P_{r1}	282.8427	282.8427	110.5000
P_{r2}	-282.8427	282.8427	110.5000
P_{r3}	-282.8427	-282.8427	110.5000
P_{r4}	282.8427	-282.8427	110.5000

6.1.2 Measurements

There were three limitations that are faced during the selection of the poses to be measured:

1. The first joint angle is bounded at 120° rose from the robot workcell conditions.
2. Leica LTD 500 Laser Tracker requires the z-axis of the T-Mac probe to be aligned with the sensor by an angle of less than 45°.
3. The laser beam from the Leica LTD 500 Laser Tracker reaching to the reflector on the T-Mac should not be interrupted while the robot is moving from one pose measurement configuration to the other.

The first and the second conditions are straightforward to check and satisfy while the third condition requires the robot trajectory between the consecutive measured poses to also satisfy the second condition.

In order to meet these conditions, paths to be followed by the robot end-effector are defined in the joint space. The firs path is defined using 64 pose measurements and extended to 200 measurements by selecting additional poses on the path. The second path is defined using 84 pose measurements and extended to 325 by again selecting additional poses on the path. The selected poses for the first and the second set of measurements are shown in Figure 6.6 and 6.7, respectively.

The measurements from the first set and the second set are taken two months apart, during which time the robot is continued to be used and even some parts of the robot are replaced. The only nominal parameter of the robot that is changed while the second set of measurements were taken is the d_7 resulting from the removal of the 5 mm washers that were between the T-Mac probe and the robot end-effector. Thus, the nominal value of the d_7 parameter is taken

as 106.5 mm for the first set of measurements while taken as 101.5 mm for the second set on the parameter identification stage.

The measurements are taken by using a code written in Visual Basic together with the related functions of emScon Software Development Kit (SDK) of Leica Laser Tracker. The Visual Basic for Applications (VBA) inside Microsoft Excel 2007 is used for both creating a basic GUI and for storing the associated measurement data on the worksheets. This proved to be useful for taking the measurements rapidly and loading these measurements to the designed kinematic calibration GUI discussed in Appendix A.

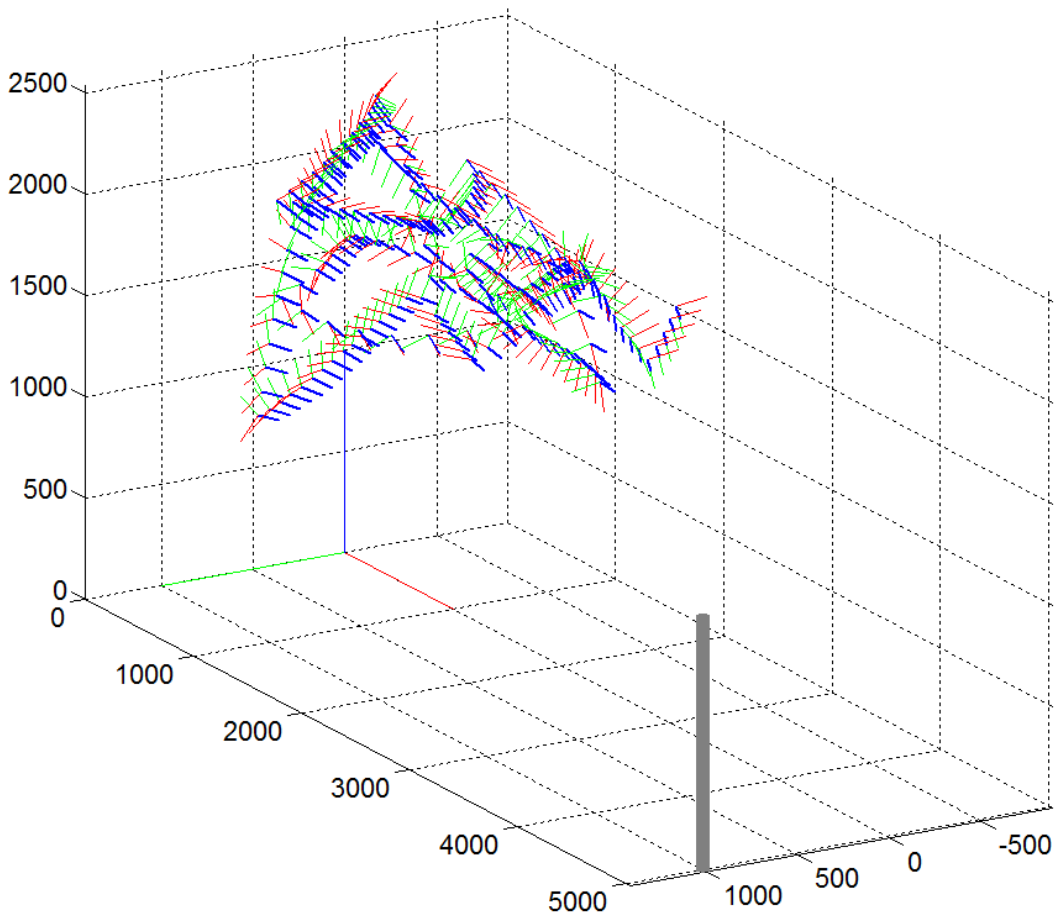

Figure 6.6: The first set of 200 measurements according to the robot base coordinate system. The measurement system is represented by the gray cylinder. The blue lines show the orientation of the z-axes of the poses.

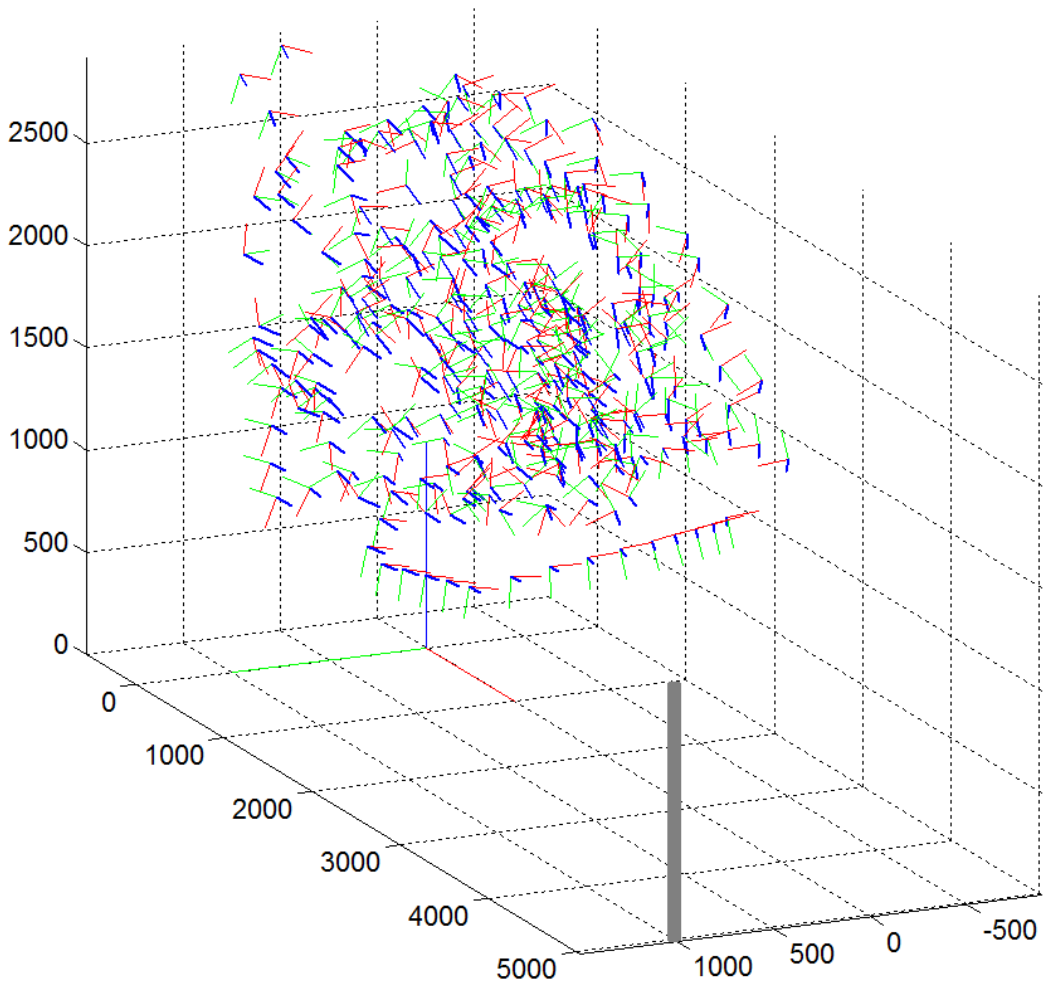

Figure 6.7: The second set of 325 measurements according to the robot base coordinate system. The measurement system is represented by the gray cylinder. The blue lines show the orientation of the z-axes of the poses.

6.1.3 Robot Program

In order to instruct the robot to the joint angle configurations, a robot controller code is written using RAPID language [47]. Each corresponding joint angle configuration is first assigned a to a robot joint target variable using the *jointtarget* data type as [47]:

```
CONST jointtarget JointTarget_number:=[[joint angles],[external axes]];
```

where the *joint angles* and the *external axes* locations are written in order and separated by a comma [47]. These joint targets are then used inside the *MoveAbsJ* command [47]:

```
MoveAbsJ JointTarget_number,v80,fine,Tool_TMac;
```

where *v80* is the selected *speeddata* variable which corresponds to 80mm/s speed for the TCP and *fine* is the *zonedata* variable which means the joint angle values are instructed without any flyby or tolerance value [47]. *Tool_TMac* is the *tooldata* variable that is defined inside the code for the T-Mac as [47]:

```
PERS tooldata Tool_TMac:=[TRUE,[Position],[Orientation]],
```

where *TRUE* indicates that the robot is holding the tool and the *Position* and *Orientation* are the translation and rotation of the tool coordinate system with respect to robot wrist coordinate system of the robot in mm and quaternion, respectively.

6.2 Results

The optimal pose selection algorithm is applied on both sets of measurements and 30 poses are selected from each of the set. The measurements for these selected poses are used on the identification stage to obtain the estimated errors on the parameter values. The remaining poses are used to evaluate the pose accuracy of the robot before and after the identification.

The resultant estimated errors on parameters using the selected poses of the first set of measurements are given in Table 6.3. The high value of the estimated error of the parameter d_1 can be explained by the differences of the reference guide holes towards the z axis of the base coordinate system. The estimated error of the parameter θ_6 also includes the orientation error about z axis of the end effector frame and thus, the error associated with the mounting of the T-Mac probe to the robot. This is also the case for the parameter α_7 which is the orientation error about x axis of the end-effector frame. The large estimated error of the parameter θ_2, θ_4 and θ_5 shows the offsets of the joint angle encoder values. The error on the parameter θ_2 was an expected error since the part related to the second joint was reported to be replaced prior to the experiment. There are also large errors on the third link parameters a_4, d_4, α_4 and θ_4 which might be resulted from the effects of heavy loads.

The resultant estimated errors on parameters using the selected poses of the second set of measurements are given in Table 6.4. The robot is put under maintenance after the first set

Table 6.3: The estimated errors of the parameters after using selected pose measurements for the first set of measurements.

Link	a_i (μm)	d_i (μm)	α_i (mrad)	θ_i (mrad)	β_i (mrad)
1	-276	-3426	1.286	0.511	-
2	-815	-2869	-0.473	-6.465	-
3	222	-	0.134	0.295	0.132
4	1133	1207	2.120	2.445	-
5	-3	-82	1.625	0.965	-
6	13	1460	-0.703	-7.057	-
L	-246	-	-1.094	-	-

of measurements is taken. This might explain the smaller errors on some of the parameters compared to the first set results. For instance, the estimated error on the parameter θ_2 is greatly decreased. The estimated errors on some of the third link parameters are also decreased while the offset of the forth joint angle encoder is still high.

Table 6.4: The estimated errors of the parameters after using selected pose measurements for the second set of measurements.

Link	a_i (μm)	d_i (μm)	α_i (mrad)	θ_i (mrad)	β_i (mrad)
1	-874	-4028	0.857	0.471	-
2	-497	-1410	-0.048	-2.047	-
3	-78	-	0.448	-0.892	-0.125
4	-172	1462	0.523	3.257	-
5	53	469	0.007	-1.138	-
6	-443	919	-1.306	-7.628	-
L	-443	-	0.409	-	-

The pose errors of the 170 measurements of the first set and the 295 measurements of the second set that are not used on the identifications can be seen in Table 6.5 and Table 6.6, respectively. It can be seen that the pose errors are greatly reduced on both cases. The first set has larger initial errors compared to the second set that might be resulted from the larger estimated error of the θ_2 parameter on the first set.

Overall, the experiment results show that a significant improvement on the pose accuracy of the robot is achieved by using only 30 measurements. Initial positioning errors are reduced by more than 95% for the first set and 80% for the second set. The same way, initial orientation errors are reduced by more than 84% for the first set and 65% for the second set.

Table 6.5: The RMS errors of the end effector pose before and after identification with the selected measurement poses for the first set of measurements.

Pose Component	Initial Errors	Selected Poses
ΔP_X (mm)	4.31	0.14
ΔP_Y (mm)	6.61	0.07
ΔP_Z (mm)	7.65	0.15
$\Delta\gamma_X$ (mrad)	25.68	3.47
$\Delta\gamma_Y$ (mrad)	6.54	0.95
$\Delta\gamma_Z$ (mrad)	24.75	3.76

Table 6.6: The RMS errors of the end effector pose before and after identification with the selected measurement poses for the second set of measurements.

Pose Component	Initial Errors	Selected Poses
ΔP_X (mm)	2.60	0.23
ΔP_Y (mm)	2.33	0.21
ΔP_Z (mm)	1.65	0.32
$\Delta\gamma_X$ (mrad)	11.45	3.90
$\Delta\gamma_Y$ (mrad)	5.72	1.40
$\Delta\gamma_Z$ (mrad)	11.78	3.95

CHAPTER 7

CONCLUSION

Robot calibration is being researched for more than four decades, during which time several methods are proposed. In an industrial point of view, robot calibration should be performed in minimal time and with least effort to decrease the detrimental effects of the production halt. Thus, a robot calibration method needs to be efficient enough to be performed in a factory environment

Several robot calibration methods are reviewed with the above requirements in concern. Kinematic calibration is decided to be performed on the experiments since the errors associated with other parameters are minimal for the industrial robots as noted in the previous studies and also the errors on the kinematic parameters can be corrected on the robot controller without requiring any additional software or hardware. Full pose measurements from the robot are taken to decrease the time associated with the measurements by obtaining all pose information in a single measurement. Least squares optimization is used on the parameter identification stage for its fast converging characteristic.

A robot kinematic calibration graphical user interface is developed in Matlab to be used for both the simulations and the experiments by coding the necessary mathematical routines for forward geometric model and parameter identification. Identification Jacobian matrices are derived using symbolic expressions in Matlab to be used for any six DoF serial robot. This interface is further supported with additional interfaces for error correction and optimal pose selection.

Kinematic calibration simulations are performed using this interface and the improvements on the pose accuracy of the robot as a result of the calibration are obtained. Through different

measurement noise added to the pose measurements, the negative effects of the measurement noise to the parameter identification are observed. Common optimal pose selection algorithms are reviewed and a modified algorithm is presented. This algorithm is later used during the simulations and experiments.

Kinematic calibration experiments are performed on an ABB IRB 6600 industrial robot. The details of the measurement stage are presented for the collecting of the measurement data. Additional measurements are taken to validate the calibration. According to the results, the initial robot pose errors are reduced by more than 80% for the positioning components and 65% for the orientation components.

In conclusion, an efficient kinematic calibration that complies with the factory environment is presented in this study and it is further supported by simulations and experiments, using novel measurement systems and measurement selection strategies.

7.1 Future Work

The errors on non-geometric parameters are treated as measurement noise in kinematic calibration. While the effects of these parameters on the industrial robot pose accuracy is showed to be minimal, this might not be necessarily true for all robots and even amongst all industrial robots. On the other hand, a full robot calibration that combines all possible error sources is still a complex procedure and it is not practiced often. An efficient method for full robot calibration should be further researched.

Optimal pose selection for kinematic calibration is proved to be valuable in terms of getting better results with the same or even less number of measurements. On the other hand, the pose selection algorithms are still an active field of research. A global method that can be used to determine the optimal poses for different robot geometries will be instrumental for future robot calibration studies.

Self calibrating methods are not widely used on industrial robots while they eliminate the need for an external measurement system. The main challenge for these methods is their hard to apply constraints for the factory environment. A useful strategy to perform these self calibrating methods on limiting conditions of the robot workcell needs to be investigated.

REFERENCES

[1] Nof, S.Y., Ed., *Handbook of Industrial Robotics*, John Wiley & Sons Inc., New York, 1985.

[2] Whitney, D.E., Lozinski, C.A., Rourke, J.M., *Industrial Robot Forward Calibration Method and Results*, ASME Journal of Dynamic Systems, Measurment, and Control, Vol. 108, No. 1, pp. 1-8, 1986.

[3] Judd, R.P., Knasinski, A.B., *A technique to calibrate industrial robots with experimental verification*, IEEE Transactions on Robotics and Automation, Vol. 6, No. 1, pp. 20-30, 1990.

[4] Shiakolas, P.S., Conrad, K.L., Yin, T.C., *On the Accuracy, Repeatability, and Degree of Influence of Kinematics Parameters for Industrial Robots*, International Journal of Modelling and Simulation, Vol. 22, No. 3, pp. 245-254, 2002.

[5] Roth, Z.S., Mooring, B.W., Ravani, B., *An overview of robot calibration*, IEEE Journal of Robotics and Automation, Vol. 3, No. 5, pp. 377-385, 1987.

[6] Khalil, W., Dombre, E., *Modeling, Identification and Control of Robots*, Hermes Penton Science, 2002.

[7] Gong, C., Yuan, J., Ni, J., *Nongeometric error identification and compensation for robotic system by inverse calibration*, International Journal of Machine Tools and Manufacture, Vol. 40, pp. 2119-2137, 2000.

[8] Gatla, C., Lumia, R., Wood, J., Starr, G., *An Automated Method to Calibrate Industrial Robots using a Virtual Closed Kinematic Chain*, Proceedings of IEEE Transactions on Robotics and Automation, Vol. 23, No. 6, pp. 1105-1116, 2007.

[9] Bernhardt, R., Albright, S.L., Ed., *Robot calibration*, Chapman & Hall, 1993.

[10] Schröer, K., Albright, S.L., Grethlein, M., *Complete, Minimal and Model-Continuous Kinematic Models for Robot Calibration*, Robotics and Computer-Integrated Manufacturing, Vol. 13, No. 1, pp. 73-85, 1997.

[11] Everett, L.J., Driels, M.R., Mooring, B.M., *Kinematic modeling for robot calibration*, IEEE International Conference on Robotics and Automation, Vol. 1, pp. 183-189, 1987.

[12] Everett, L.J., Hsu, T.W., *The Theory of Kinematic Parameter Identification for Industrial Robots*, Transactions of ASME - Journal of Dynamic Systems, Measurement, and Control, Vol. 110, pp. 96-100, 1988.

[13] Mooring, B.W., Padavala, S.S., *The effect of kinematic model complexity on manipulator accuracy*, In Proceedings of the IEEE International Conference on Robotics and Automation, pp. 593-598, 1989.

[14] Bernhardt, R., *Approaches for commissioning time reduction*, Industrial Robot, Vol. 24, No. 1, pp. 62-71, 1997.

[15] Caenen, J.L., Angue, J.C., *Identification of Geometric and Non-geometric Parameters of Robots*, Proceedings of the 1990 IEEE International Conference on Robotics and Automation, pp. 1032-1037, 1990.

[16] Chen J., Chao, L.M., *Positioning error analysis for robot manipulators with all rotary joints*, IEEE Journal of Robotics and Automatio, Vol. RA-3, No. 6, 1987.

[17] Veitschegger, W.K., Wu, C.H., *Robot calibration and compensation*, IEEE Journal of Robotics and Automation, Vol. 4, No. 6, pp. 643-656, 1988.

[18] Jang, J.H., Kim, S.H., Kwak, Y.K., *Calibration of geometric and non-geometric errors of an industrial robot*, Robotica, Vol. 19, No. 3, pp. 311-321, 2001.

[19] Lightcap, C., Hamner, S., Schmitz, T., Banks, S., *Improved Positioning Accuracy of the PA10-6CE Robot with Geometric and Flexibility Calibration*', IEEE Transactions on Robotics, Vol. 24, No. 2, pp. 452-456, 2008.

[20] Paul, R.P., *Robot Manipulators: Mathematics, Programming, and Control*, MIT Press, 1981.

[21] Denavit, J., Hartenberg, R.S., *A Kinematic Notation for Lower-Pair Mechanisms based on Matrices*, ASME Journal of Applied Mechanics, Vol. 77, pp. 215-221, 1955.

[22] Hayati, S.A., Mirmirani, M., *Improving the absolute positioning accuracy of robot manipulators*, J. Robot. Syst. Vol. 2, pp. 397-413, 1985.

[23] Robertson, A.P., Dumont, C., *Design of Robot Calibration Models Using Genetic Programming*, International Symposium on Robotics and Automation Conference, Mexico, 2002.

[24] Dolinsky, J.U., Jenkinson, I.D., Colquhoun, G.J., *Application of genetic programming to the calibration of industrial robots*, Computers in Industry, Vol. 58, No. 3, pp. 255-264, 2007.

[25] Wang, D., Bai, Y., *Improving position accuracy of robot manipulators using neural networks*, Proceedings of the IEEE Instrumentation and Measurement Technology Conference, Ottawa, 2005.

[26] Alici, G., Shirinzadeh, B., *Laser interferometry based robot position error modeling for kinematic calibration*, Proceedings of the IEEE/RSJ Int. Conference on Intelligent Robots and Systems, 2003.

[27] Watanabe, A., Sakakibara, S., Ban, K., Yamada, M., Shen, G., *A Kinematic Calibration Method for Industrial Robots Using Autonomous Visual Measurement*, Annals of the CIRP, Vol. 55, pp. 1-6, 2006.

[28] Hidalgo, F., Brunn, P., *Robot Metrology and Calibration Systems - A Market Review*, Industrial Robot, Vol. 25, No. 1, pp. 42-47, 1998.

[29] Khalil, W., Besnard, S., Lemoine, P., *Comparison study of the geometric parameters calibration methods*, Int. Journal of robotics and Automation, Vol. 15, No. 2, pp. 56-67, 2000.

[30] Seber, G.A.F., Wild, C.J., *Nonlinear Regression*, John Wiley and Sons, New York, 1989.

[31] Hollerbach, J.M., Khalil, W., Gautier, M., *Model Identification*, Chapter in the Book: Springer Handbook of Robotics, pp. 321-344, Springer, 2008.

[32] Levenberg, K., *A Merhod for the Solution of Certain Non-Linear Problems in Least-Squares*, Quarterly of Applied Mathematics-Notes 2, pp. 164-168, 1944.

[33] Marquardt, D.W., *An Algorithm for Least-Squares Estimation of Nonlinear Parameters*, Journal of the Society for Industrial and Applied Mathematics, Vol. 11, No. 2, pp. 431-441, 1963.

[34] Liu, Y., Liang, B., Qiang, W., Jiang, Y.S., *Improvement on Robots Positioning Accuracy based on Genetic Algorithm*, IMACS Multiconference on Computational Engineering in Systems Application, 2006.

[35] Zhuang, H., Wang, K., Roth, Z.S., *Optimal Selection of Measurement Configurations for Robot Calibration Using Simulated Annealing*, Proceedings of IEEE International Conference on Robotics and Automation, pp. 393-398, 1994.

[36] Driels, M.R., Pathre, U.S., *Significance of observation strategy on the design of robot calibration experiments*, Journal of Robotic Systems, Vol. 7, No. 2, pp. 197-223, 1990.

[37] Borm, J.H., Menq, C.H., *Determination of Optimal Measurement Configurations for Robot Calibration based on Observability Measure*, International Journal of Robotics Research, Vol. 10, No .1, pp. 51-63, 1991.

[38] Nahvi, A., Hollerbach, J.M., *The Noise Amplification Index for Optimal Pose Selection in Robot Calibration*, Proceedings of IEEE International Conference on Robotics and Automation, Minneapolis, 1996.

[39] Sun, Y., Hollerbach, J.M., *Observability Index Selection for Robot Calibration*, Proceedings of the IEEE International Conference on Robotica and Automation, Pasadena, 2008.

[40] Zhuang, H., Wu, J., Huang, W., *Optimal Planning of Robot Calibration Experiments by Genetic Algorithms*, Proceedings of IEEE International Conference on Robotics and Automation, Minneapolis, Minnesota, pp. 981-986, April 1996.

[41] Mitchell, T.J., *An algorithm for the construction of D-optimal experimental designs*, Technometrics, Vol. 16, pp. 203-210, 1974.

[42] Sun, Y., Hollerbach, J.M., *Active Robot Calibration Algorithm*, IEEE International Conference on Robotics and Automation, Pasadena, pp. 1276-1281, 2008.

[43] Craig, J.J., *Introduction to Robotics*, Addison-Wesley, 1989.

[44] ABB, *Product specification*, 3HAC 14064-1 Rev.H, 2004.

[45] Leica, *Leica Laser Tracker System*, 1999.

[46] Leica, *PCMM System Specifications: Leica Absolute Tracker and Leica T-Products*, 2010.

[47] ABB, *RAPID reference manual*, 3HAC 7783-1 Rev.C, 2004.

APPENDIX A

GRAPHICAL USER INTERFACE

In order to use for the kinematic calibration experiments and simulations, a graphical user interface (GUI) is designed in MATLAB. The options and the features of this GUI are explained in detail together with its use in later sections.

A.1 Kinematic Calibration Interface

A.1.1 Main Window

The **Main Window** of the GUI can be seen in Figure A.1. There are four regular buttons and two radio buttons on this window. The two radio buttons are:

- Simulation
- Application

Three regular buttons, Kinematic Parameters, Measurements and Optimization Settings, opens their respective window according to the setting of these radio buttons. In other words, windows designed for simulation will pop up if Simulation radio button is selected and windows designed for application will pop up if Application radio button is selected. Start Calibration button is the final button to be pushed when all the required information are filled on the other windows.

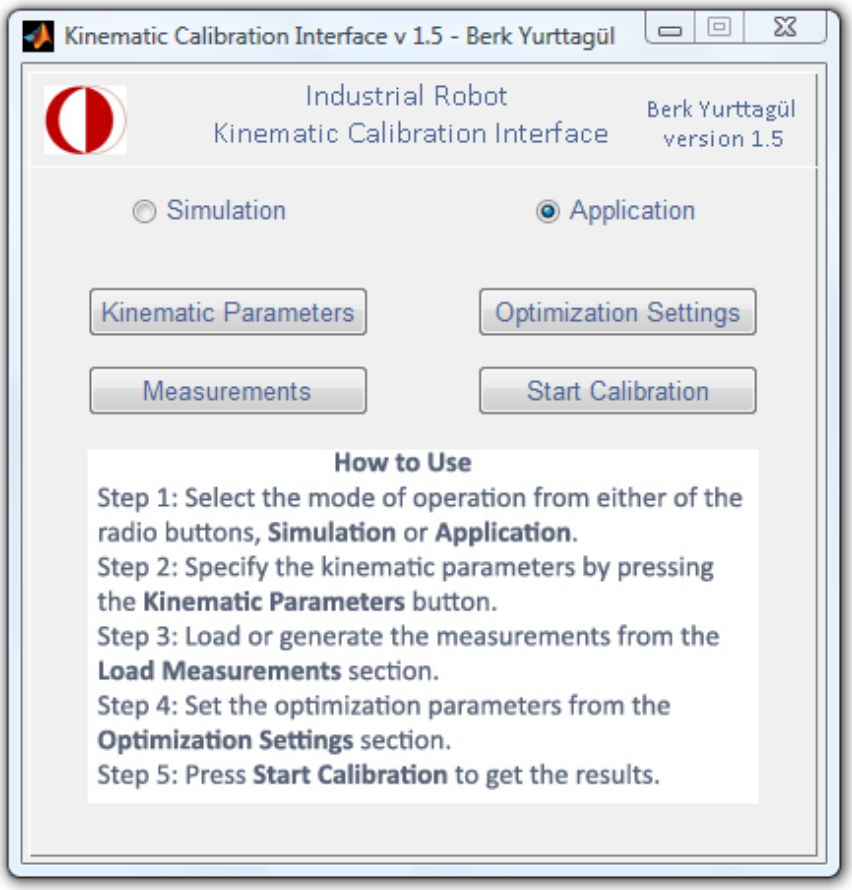

Figure A.1: The Main window.

A.1.2 Kinematic Parameters Window

The **Kinematic Parameters Window** of the GUI is designed to specify and display the parameters of the kinematic model. This is done by filling the empty field with the value of the respective parameters. Link lengths and offsets should be specified in millimeters while link twist and joint angles should be specified in radians. In simulation mode, both the nominal values of the kinematic parameters and the specified deviation are needed to be filled on this window. This can be seen in can be seen in Figure A.2. Application mode evidently requires only the nominal values of the kinematic parameters as seen in Figure A.3. These specified parameters can be saved using the Save button and these saved parameters can be loaded using the Load button. The Accept button updates the values of the parameters according to the changes while the Cancel button discards all changes and returns the previous values of the parameters specified before.

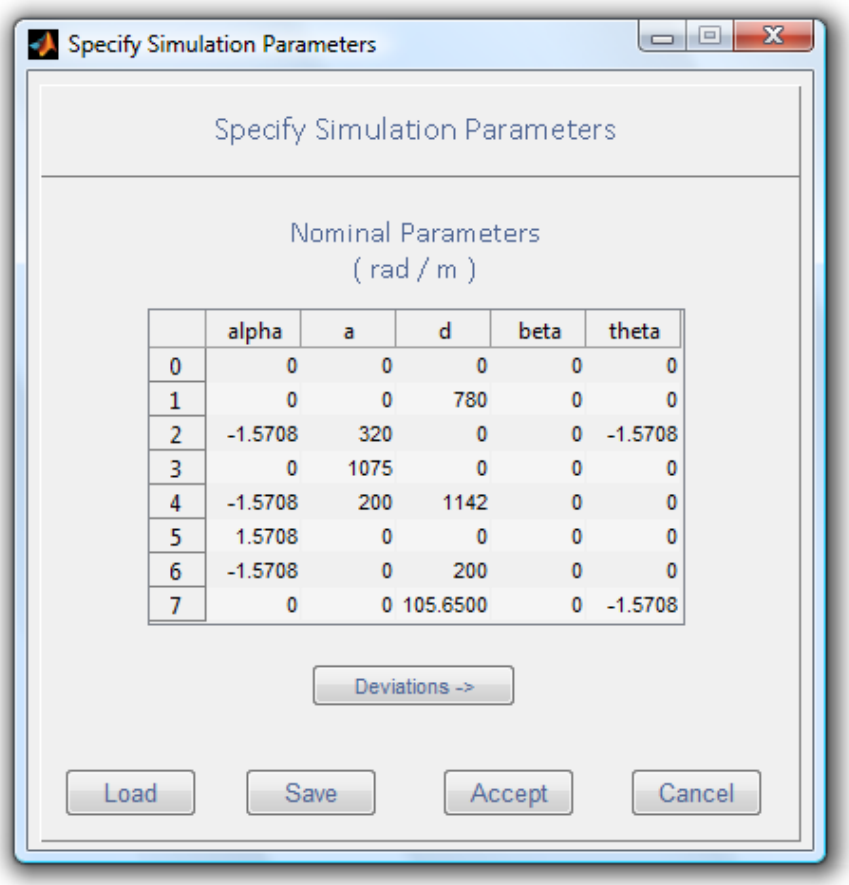

	alpha	a	d	beta	theta
0	0	0	0	0	0
1	0	0	780	0	0
2	-1.5708	320	0	0	-1.5708
3	0	1075	0	0	0
4	-1.5708	200	1142	0	0
5	1.5708	0	0	0	0
6	-1.5708	0	200	0	0
7	0	0	105.6500	0	-1.5708

Figure A.2: The Kinematic Parameters window in simulation mode.

A.1.3 Measurements Window

Measurements Window of the GUI is designed to specify and display measurements related data. This is done by filling the empty field with the value of the respective parameters. Positions should be specified in millimeters while orientation and joint angles should be specified in radians. In application mode, this window only changes or displays the pose measurements and the corresponding standard deviation and joint angle values as seen in Figure A.4. In simulation mode, this window additionally displays the measured, calculated and actual pose measurements as can be seen in Figure A.5.

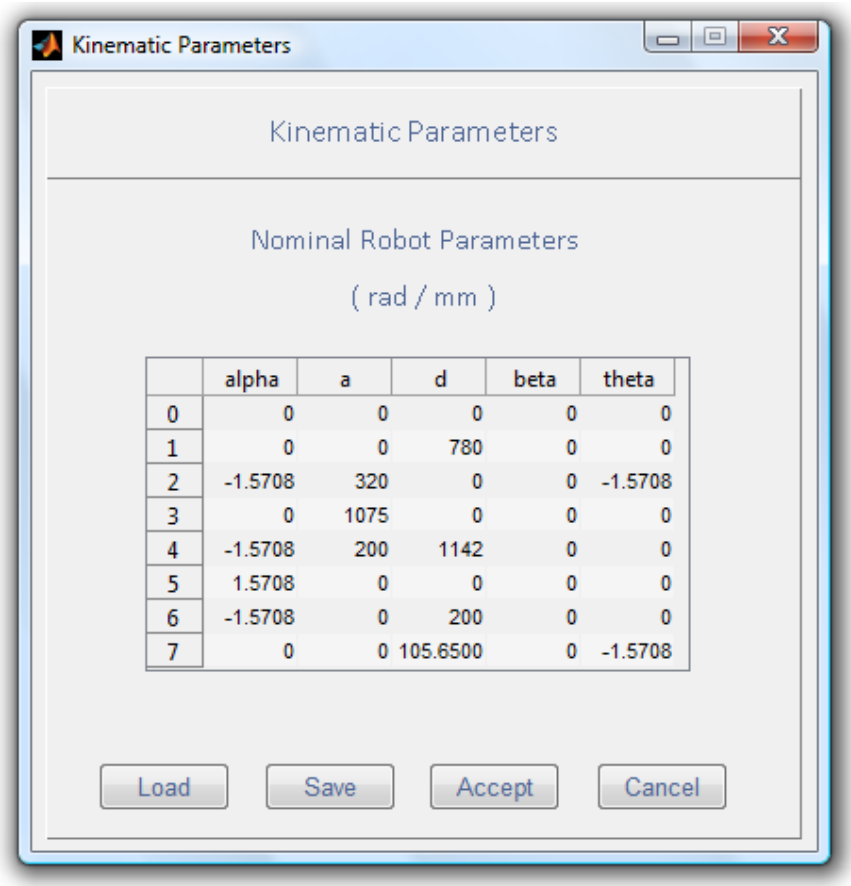

	alpha	a	d	beta	theta
0	0	0	0	0	0
1	0	0	780	0	0
2	-1.5708	320	0	0	-1.5708
3	0	1075	0	0	0
4	-1.5708	200	1142	0	0
5	1.5708	0	0	0	0
6	-1.5708	0	200	0	0
7	0	0	105.6500	0	-1.5708

Figure A.3: The Kinematic Parameters window in application mode.

A.1.3.1 Generate / Load Joint Angles Window

Generate / Load Joint Angles Window can be seen in Figure A.6. This window can be used to generate random joint angle configurations according the range of movement of the joints or load the joint angle data. The upper and lower bounds of the joints can be specified by filling the respective fields. The number of measurements can be specified by selecting the particular number on the drop down list. Pressing the Generate button will close this window and update the **Measurements Window** with the updated measurements. These joint angles are used to calculate the nominal pose data using the nominal parameters and the actual pose data using the deviated parameters. The measured pose data is calculated by adding the generated or the loaded measurement noise to the actual pose data where the measurement noise is taken from the **Generate / Load Measurement Noise Window**. The generated joint angle configurations can be saved using the Save button and this saved data can be loaded

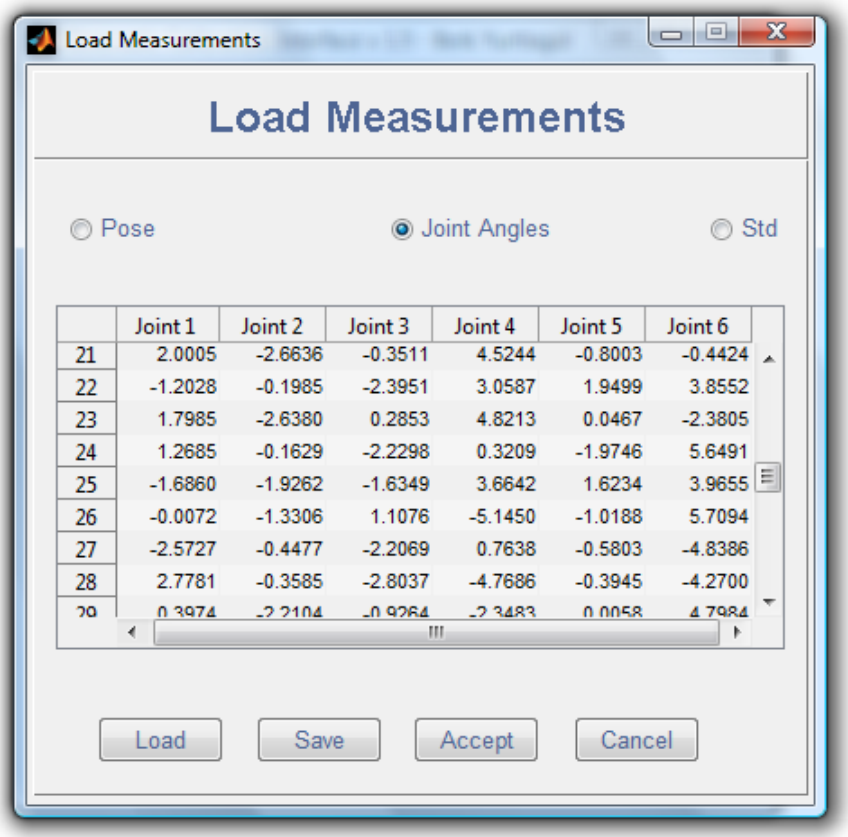

	Joint 1	Joint 2	Joint 3	Joint 4	Joint 5	Joint 6
21	2.0005	-2.6636	-0.3511	4.5244	-0.8003	-0.4424
22	-1.2028	-0.1985	-2.3951	3.0587	1.9499	3.8552
23	1.7985	-2.6380	0.2853	4.8213	0.0467	-2.3805
24	1.2685	-0.1629	-2.2298	0.3209	-1.9746	5.6491
25	-1.6860	-1.9262	-1.6349	3.6642	1.6234	3.9655
26	-0.0072	-1.3306	1.1076	-5.1450	-1.0188	5.7094
27	-2.5727	-0.4477	-2.2069	0.7638	-0.5803	-4.8386
28	2.7781	-0.3585	-2.8037	-4.7686	-0.3945	-4.2700
29	0.3974	-2.2104	-0.9264	-2.3483	0.0058	4.7984

Figure A.4: The Measurement window in application mode.

using the Load button. The Accept button updates the joint angle configurations according to the changes while the Cancel button discards all changes and returns the previous joint angle configurations specified before.

A.1.3.2 Generate / Load Measurement Noise Window

Generate / Load Measurement Noise Window can be seen in Figure A.7. This window can be used to generate random measurement noise according to the selected measurement system specifications. The measurement system can be selected from the drop down list on the top of the window. Pressing Generate button generates measurement noise and fills the table with this information. The generated measurement noise data can be saved using the Save button and this saved data can be loaded using the Load button. The Accept button updates

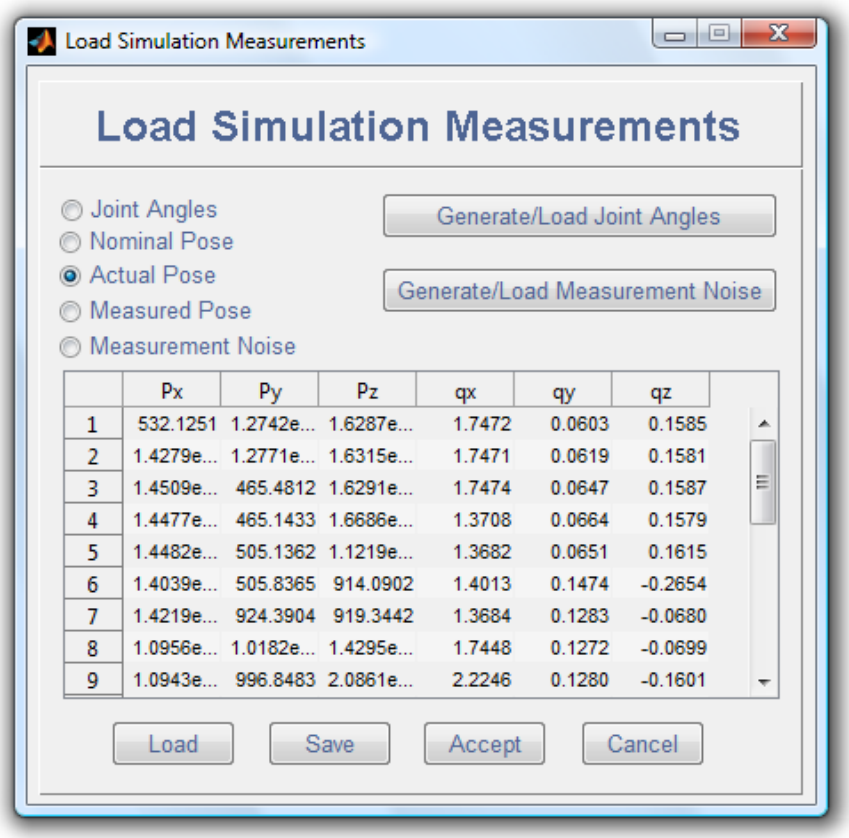

	Px	Py	Pz	qx	qy	qz
1	532.1251	1.2742e...	1.6287e...	1.7472	0.0603	0.1585
2	1.4279e...	1.2771e...	1.6315e...	1.7471	0.0619	0.1581
3	1.4509e...	465.4812	1.6291e...	1.7474	0.0647	0.1587
4	1.4477e...	465.1433	1.6686e...	1.3708	0.0664	0.1579
5	1.4482e...	505.1362	1.1219e...	1.3682	0.0651	0.1615
6	1.4039e...	505.8365	914.0902	1.4013	0.1474	-0.2654
7	1.4219e...	924.3904	919.3442	1.3684	0.1283	-0.0680
8	1.0956e...	1.0182e...	1.4295e...	1.7448	0.1272	-0.0699
9	1.0943e...	996.8483	2.0861e...	2.2246	0.1280	-0.1601

Figure A.5: The Measurement window in simulation mode.

the measurement noise data according to the changes while the Cancel button discards all changes and returns the previous measurement noise data specified before. These specified measurement data can be saved using the Save button and this saved data can be loaded using the Load button. The Accept button updates the measurement data according to the changes while the Cancel button discards all changes and returns the previous measurement data specified before.

A.1.4 Optimization Settings Window

Optimization Settings Window can be seen in Figure A.8. This window can be used to specify the parameters to be included on the parameter identification stage and the identification algorithm as well as the maximum number of iterations and the tolerance values of the identification algorithm. The parameters can be removed from the identification by simply se-

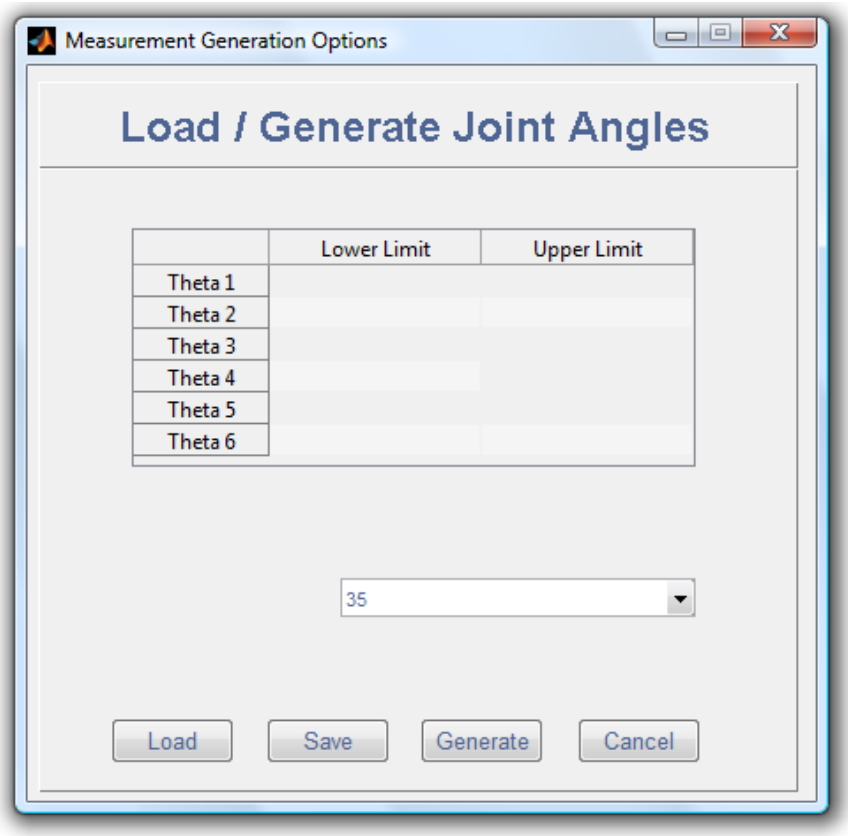

Figure A.6: Generate / Load Measurements window.

lecting them from the list. Multiple parameters can be selected by pressing the Ctrl key. The maximum number of iterations specifies how many times the algorithm will iterate at most. The termination tolerance of the function specifies the value of the calculated least squares from Eq 4.3 to be reduced for the algorithm to stop. The same way, the termination tolerance of the parameters specifies the value of the deviation on each parameter from Eq 4.8 to be reduced for the algorithm to stop.The two identification algorithms that can be selected using the radio buttons on the right top place of the window are Gauss - Newton and the Matlab function *lsqnonlin*. These specified parameters can be saved using the Save button and these saved parameters can be loaded using the Load button. The Accept button updates the values of the parameters according to the changes while the Cancel button discards all changes and returns the previous values of the parameters specified before.

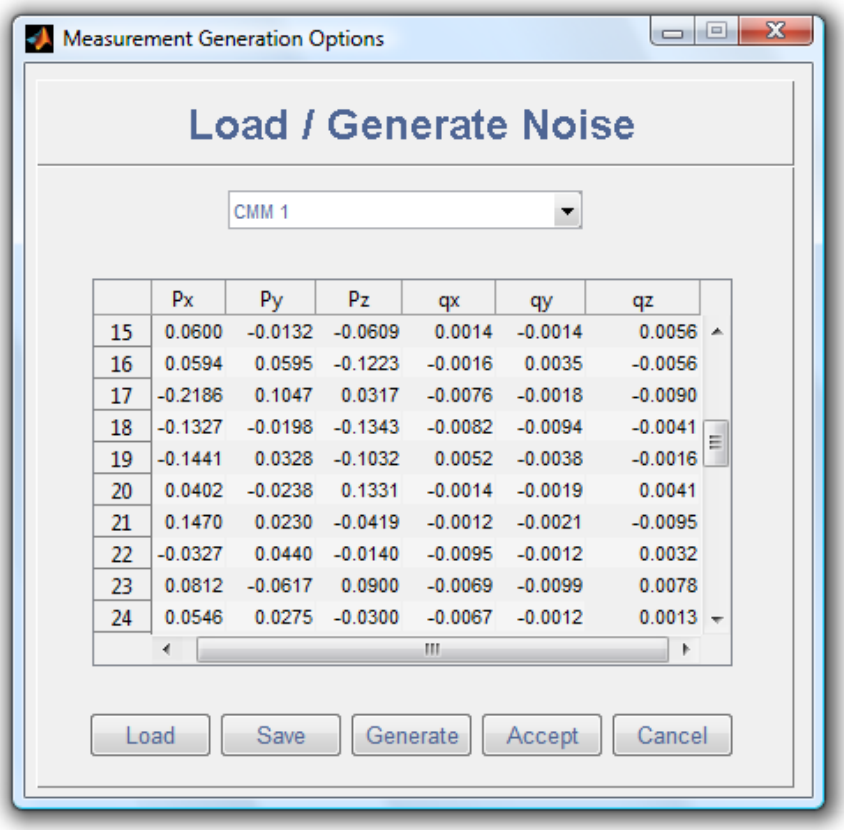

	Px	Py	Pz	qx	qy	qz
15	0.0600	-0.0132	-0.0609	0.0014	-0.0014	0.0056
16	0.0594	0.0595	-0.1223	-0.0016	0.0035	-0.0056
17	-0.2186	0.1047	0.0317	-0.0076	-0.0018	-0.0090
18	-0.1327	-0.0198	-0.1343	-0.0082	-0.0094	-0.0041
19	-0.1441	0.0328	-0.1032	0.0052	-0.0038	-0.0016
20	0.0402	-0.0238	0.1331	-0.0014	-0.0019	0.0041
21	0.1470	0.0230	-0.0419	-0.0012	-0.0021	-0.0095
22	-0.0327	0.0440	-0.0140	-0.0095	-0.0012	0.0032
23	0.0812	-0.0617	0.0900	-0.0069	-0.0099	0.0078
24	0.0546	0.0275	-0.0300	-0.0067	-0.0012	0.0013

Figure A.7: Generate / Load Measurement Noise window.

A.1.5 Displaying the Results

Pressing the Start Calibration button starts the parameter identification and displays the value of the sum of squares of the error for each iteration on the command window. When either one of the conditions stated on the **Optimization Settings Window** is met, the algorithm stops and the results are displayed as in Figure A.9. On application mode, the results are the estimated errors on parameters and the final estimated parameters. On simulation mode, the estimation error of the algorithm is also displayed. These results are shown in the **Main Window** and written on the command window at the same time.

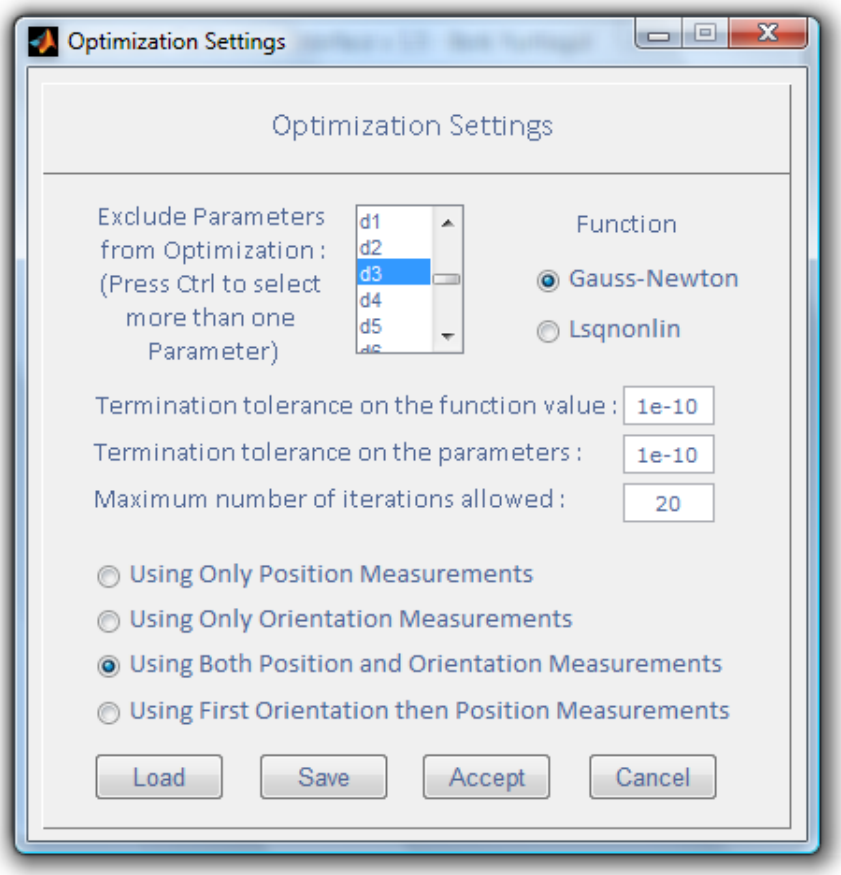

Figure A.8: The Optimization Settings window.

A.2 Pose Selection Interface

The **Pose Selection Interface** of the GUI can be seen in Figure A.10. There are four radio buttons on this window. The two radio buttons for different initial set of measurements are:

- Random IS: The algorithm uses a randomly selected initial set from the candidate set.
- Decreased IS: The algorithm uses a selected initial set using the first step of the algorithm discussed in Section 4.3.

The two radio buttons for different algorithms are:

- Detmax: Detmax algorithm is used for the pose selection as discussed in Section 4.3.

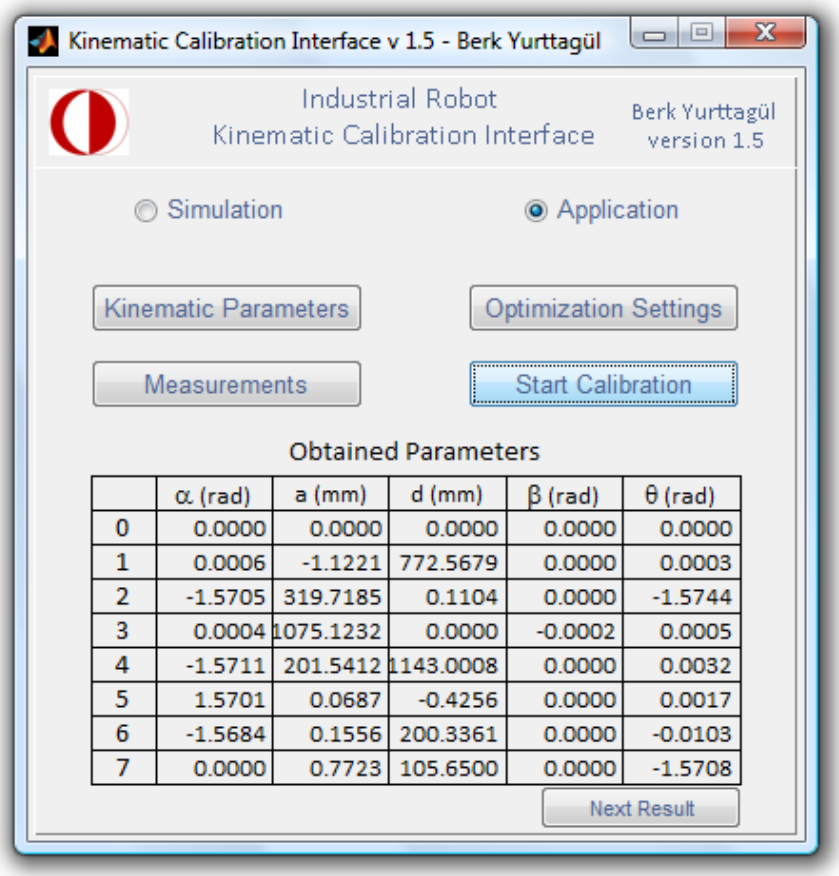

	α (rad)	a (mm)	d (mm)	β (rad)	θ (rad)
0	0.0000	0.0000	0.0000	0.0000	0.0000
1	0.0006	-1.1221	772.5679	0.0000	0.0003
2	-1.5705	319.7185	0.1104	0.0000	-1.5744
3	0.0004	1075.1232	0.0000	-0.0002	0.0005
4	-1.5711	201.5412	1143.0008	0.0000	0.0032
5	1.5701	0.0687	-0.4256	0.0000	0.0017
6	-1.5684	0.1556	200.3361	0.0000	-0.0103
7	0.0000	0.7723	105.6500	0.0000	-1.5708

Figure A.9: The results shown in the main window after pressing the Start Calibration button.

- Decreased IS: Modified version of the Detmax algorithm is used for the the pose selection as presented in Section 4.3

The number of measurements on the candidate set and the selected set are specified by filling the empty fields with the value of the respective parameters. The model parameters are also specified by filling the empty fields that appear by pressing the DH Parameters button. Pressing the Start button asks the user if the user wants to load a candidate set or the candidate set will be generated by the interface.

The graphic below is updated each time the observability index is increased. The blue dot represents the observability index value of the initial set, red dots represent the increases made by the Detmax algorithm and the green dots represents the increases made by the modified algorithm.

After the algorithm stops and the resultant set of measurements are obtained, the interface asks the user if the measurements will be saved. Algorithm saves the resultant measurements and the candidate set on a Microsoft Excel worksheet file specified by the user.

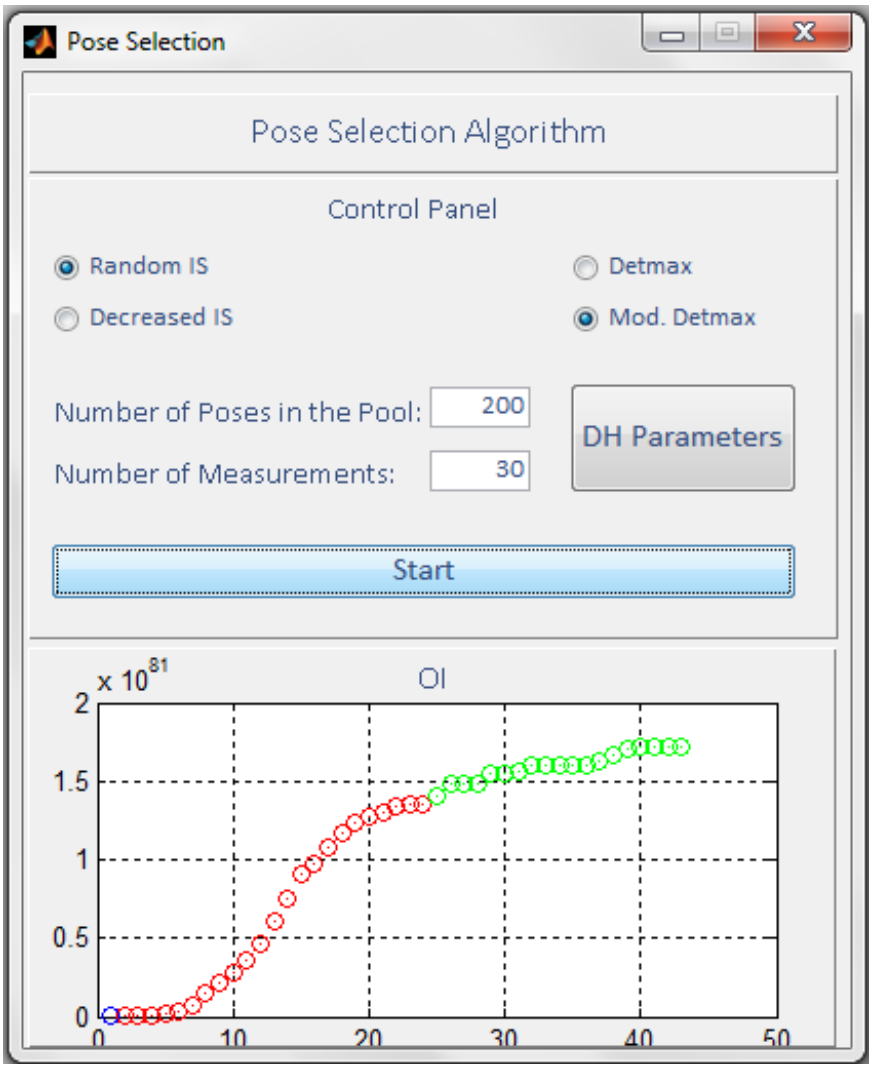

Figure A.10: The Pose Selection Interface.